Available on CMS information server

CMS NOTE 2003/025

The Compact Muon Solenoid Experiment

CMS Note

Mailing address: CMS CERN, CH-1211 GENEVA 23, Switzerland

October 6, 2003

Test-Beam Analysis of the Effect of Highly Ionising Particles on the Silicon Strip Tracker

W. Adam
Institut für Hochenergiephysik der OeAW, Wien, Austria
W. Beaumont, V. Zhukov
Universitaire Instelling Antwerpen, Wilrijk, Belgium
D. Contardo, N. Lumb, L. Mirabito, S. Peries, B. Trocme
IPNL, Université Claude Bernard, Lyon, France
F. Drouhin, L. Gross, D. Vintache
IN2P3-CNRS-ULP, LEPSI Strasbourg, UHA Mulhouse, Strasbourg, France
B. Wittmer, J. Olzen
RWTH, I. Physikalisches Institut, Aachen, Germany
M. Fahrer
Institut für Experimentelle Kernphysik, Karlsruhe, Germany
N. De Filippis, D. Giordano, S. My, L. Silvestris
INFN and Università Bari, Italy
V. Ciulli, S. Paoletti
INFN and Università, Firenze, Italy
C. Zucchetti, L. Servoli
INFN and Università, Perugia, Italy
J. Bernardini, T. Boccali, M. D'Alfonso, R. Dell'Orso, S. Dutta, A. Giassi, S. Gennai, A. Kyriakis[1),]
F. Palla, F. Rinaldi, A. Rizzi, P. G. Verdini
INFN, Università and Scuola Normale Superiore, Pisa, Italy
P. Bartalilni,R. Chierici, P. Siegrist, A. Tsirou
CERN, Geneva, Switzerland
R. Bainbridge, N. Marinelli[2)]
Blackett Laboratory, Imperial College, London, UK
I. Tomalin
Rutherford Appleton Laboratory, Chilton, UK

1) now at Institute of Nuclear Physics "Demokritos", Attiki, Greece

2) now at Institute of Accelerating Systems and Applications (IASA) and University of Athens, Greece

Abstract

Highly Ionizing Particles (HIPs) created by nuclear interactions in the tracker sensors produce large signals which can momentarily saturate an APV readout chip. This phenomenon is studied in two different beam-tests performed at PSI and X5 in 2002. The probability of a HIP-like event occurring per incident pion is measured, as is the time required for an APV to recover from such an event. Distortions induced in the APV baseline are also studied. From these results, the expected inefficiency of the CMS Tracker due to HIPs is inferred. The dependence of the results on the APV's configuration parameters and inverter stage resistor value is shown.

1 Introduction

During the beam test performed in October 2001 at the CERN X5 beam line [1], where six modules of silicon detector prototypes for the CMS tracker were exposed to 120 GeV pions, a few anomalous events were observed, where, following a high energy release inside a silicon sensor, the readout front-end electronics saturates. Typically, strips collecting the energy release give a large, positive signal, whereas the outputs of all other channels connected to the same APV25 readout chip[5], are driven down to a level well below their normal pedestals. The energy release can be large enough to saturate not only those channels in the APV which collect the signal but also all the other channels in the APV which can be driven down to the APV digital 0 level[1)]. A typical event is shown in Fig. 1. The saturation typically persists for a few hundred nanoseconds, after which the baseline recovers to its normal level, (possibly overshooting before doing so). This can result in temporary inefficiency of all the APV channels. The rate observed in the October 2001 X5 beam test, for the occurrence of this kind of events is order of 10^{-4} per TOB module per incident particle [1].

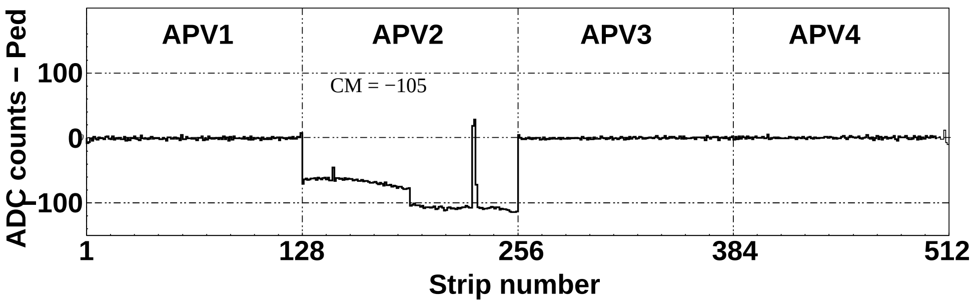

Figure 1: *Pedestal subtracted ADC counts of the four APVs in a TOB module as a function of the strip number. The second chip shows the distribution following the passage of a HIP particle. The cluster on the right hand side of APV25 consists of several fully saturated strips. The large negative common mode value (CM) is also shown in the picture.*

The saturation phenomenon has been reproduced in laboratory tests [2] and its temporal structure studied. It can be attributed to crosstalk effects caused by signals exceeding the normal operating range of the APV amplifiers by several orders of magnitude, but the effect is also enhanced by the APV powering scheme, where an inverting stage between the charge and shaping amplifier stages is powered from the 2.5 Volt supply rail via a resistor $\mathrm{R_{inv}}$, common to all 128 channels. This resistor, known as the "inverter resistor" has a default value (in 2002) of 100 Ω. During normal operation a beneficial effect of this resistor is to provide a feedback mechanism resulting in an effective on-chip common mode noise subtraction. In the laboratory tests it was found that the APV recovery time, following the injection of very large signals, depends on the value of $\mathrm{R_{inv}}$.

[1)] When there is no data to read out, the APV output is at the logic 0 level. A data frame consists of differential digital levels, defined by an output current of $\pm$ 4mA, followed by 128 samples of analogue data, where a silicon MIP equivalent signal should be represented by a current of $\pm$ 100 μA. The analogue baseline may be adjusted to give optimal dynamic range in the signal polarity in which the chip is working.

The high energy releases in the silicon sensors can be explained by the occurrence of inelastic nuclear interactions, accompanied by the creation of showers and/or highly ionizing debris. For this reason these events are called ”HIP events” (after ”Highly Ionizing Particles”), and this name is used generically throughout this note to refer to all events where a clear shift in the baseline of the APV channels is observed.

This note reports the measurements from a dedicated beam test, performed with 300 MeV/c momentum pions and protons at the “piM1” PSI beam test facility during May 2002 (with a beam time-structure close to that expected at the LHC) and from a second beam test with 120 GeV pions performed at X5 during August 2002.

The note is structured as follows. The following Section describes the experimental set-up and data acquisition system. In Sect. 3 the HIP rate measurements are presented. Section 4 examines how rapidly the APV baseline recovers following a HIP and studies the distortions in the baseline which are seen during this recovery. Section 5 presents measurements, based on reconstruction of tracks from MIP particles, of the time required for the APV efficiency to recover following a HIP. Finally, Sect.6 examines the implications of HIP events for the expected performance of the CMS Tracker.

2 The experimental setup and data acquisition system

2.1 The PSI beam test

On the basis of Monte Carlo simulations [6], the most common source of HIP events in the CMS Tracker will be the low-energy pions in minimum-bias events. This is why the 300 MeV/c pion beam located at the proton accelerator, Paul Scherrer Institut, Villigen, Switzerland (PSI) has been chosen to perform the dedicated test. The 300 MeV/c corresponds both to the most probable momentum of particles seen in LHC minimum-bias events and to the maximum of the nuclear interaction cross-section. It is also the momentum allowing the PSI beam to reach its maximum intensity.

2.1.1 The PSI beam

The beam used was the piM1 which is a high resolution pion beam line, with a momentum range between 100 and 500 MeV/c and can be operated in both polarities, thus giving access to π^-, π^+ and protons of 300 MeV/c momentum. (For protons this corresponds to about 50 MeV kinetic energy).

2.1.2 The experimental setup

Twelve new, non-irradiated modules were exposed simultaneously on the beam line. These modules came from prototype series produced at the beginning of 2002 and were equipped with the most recent parts available and as close as possible to the modules to be used in the CMS Silicon Tracker.

The beam successively crossed three Tracker Internal Barrel (TIB) type modules, three Tracker End Cap (TEC) type modules and six Tracker Outer Barrel (TOB) modules. Each of the 12 modules had 512 channels and was thus read by four APVs. As the APV recovery to normal regime depends on the value R_{inv} of the inverter resistor (see Sect. 1), beside the nominal $R_{inv} = 100\ \Omega$ resistor value, several modules were equipped with reduced resistor values of $R_{inv} = 50\ \Omega$ and one module with $R_{inv} = 75\ \Omega$.

The three TIB modules had a size of 11.9×6.3 cm^2, a thickness of 320 μm and a 120 μm readout pitch. Two modules were made out of two sensors from the CSEM company, while a third one came from the Hamamatsu company. The first and the third modules downstream of the beam had the hybrids equipped with nominal $100\ \Omega$ resistors. The operational voltage was 300 V. The second one (Hamamatsu) was operated at 240 V and was equipped with a FRF4 hybrid prototype and modified $50\ \Omega$ resistors. Due to problems in the transportation, the two central APVs of the first module were unbonded, and correspondingly not used in the analysis.

The three TEC modules were standard ring 6 (W6A+B) of trapezoidal shape (of width 8.3–10.5 cm of height 18.7 cm) with varying pitch (from 163 to 204 μm) modules from the milestone production with sensors of 500 μm thickness from Hamamatsu Company. Out of the three modules only one had dead channels (one dead and one noisy and disconnected). The depletion voltages were about 100 V, and the operating voltage at PSI was 150 V. The currents drawn ranged from $<1\mu$A up to 3μA. All three modules were left with nominal $R_{inv} = 100\ \Omega$ resistors.

The six TOB modules from the milestone production were standard TOB single layer type (18.9×9.65 cm^2) made with sensors of 500 μm thickness from the ST company with 183 μm readout pitch. The first, the second, the third and the fifth modules downstream of the beam were equipped with modified R_{inv} resistors of respectively 50, 50, 75 and 50 Ω. The fourth and the sixth modules were left with nominal $100\ \Omega$ R_{inv} resistors. The modules were operated with a 200 V bias.

The 12 modules, individually fixed on metallic support plates, were placed in two independent water cooled boxes in two groups of six and operated at room temperature, the cooling being used only to remove the heat from electronics. In addition to the module, each support plate carried an interface board housing the control interface to load and initialize the readout electronics and to drive the analog signals coming out from the APV along a 1.5 m copper cable up to the PC based ADC located just outside of the beam path. Only the sensors and possibly the front-end readout hybrids were left exposed to the beam, all the non radiation hard electronic interfaces were protected from the beam halo with a copper collimator. No optical link was used throughout this test and the long distance data path from the PC based ADC to the counting room was ensured with 100 Mbit Ethernet.

2.1.3 The trigger

The accelerator clock ran at 50 MHz while the front-end electronic clock at 40 MHz. The triggers were only allowed when the PSI and APV25 clocks were in phase, i.e. every 100 ns. The Trigger and Sequencer Card (TSC) developed for test set-ups of the Tracker was customized to synchronize the two clocks. Triggers were accepted only every 200 ns.

Moreover to get cleaner events a trigger pre-filter was introduced consisting of a particle veto of duration 16 PSI clocks before any accepted trigger, thus ensuring that no previous particle crossing before the one triggering could have caused spurious effects

Further, a new trigger sequence mode was introduced, generating ten APV trigger pulses for one particle trigger. It gave ten snapshots at 75 ns intervals of APV behavior following a HIP.

With the APV running in 'multi-mode' (three 25 ns time samples taken per trigger), one can get the whole 30 samples history of an APV after a HIP. Unfortunately the TSC modifications prevented a refined tuning of sampling time and this forbade running in deconvolution mode, for which the timing adjustment must be better than 5 ns.

The trigger for a particle going through the set-up, was obtained with a coincidence of the two upstream photo-multipliers viewing the same scintillation counter of 185 x 30 x 3 mm^3 contained in a metallic tube with air-aluminium light guide and minimizing material in front. An additional downstream counter (of large area) could be used in coincidence or anti-coincidence for beam studies or veto. A two threshold discriminator method was applied on the downstream counter signal in order to remove the proton contamination from the π^+ analyzed sample.

Two trigger configurations were used. In normal running to measure the HIP rate, no coincidence with the downstream counter was requested, since HIP interactions should stop particles in the detectors. However, in runs to measure the APV dead-time, an anti-coincidence with the downstream counter was required, since this enriched by a factor of two the HIP sample.

2.1.4 The control and data acquisition

The Control and Data Acquisition were PC based, using the Tracker PMC prototype cards (FEC and FED). The communication hardware was fast Ethernet and the framework used was the XDAQ package developed by the CMS DAQ group [8]. Dedicated event builder and data storage were written for this test and a distributed monitor display interface was written in Java. Technical details of this system can be found in reference [7]. For an event size of 14 KB, a maximum rate of 200 Hz was achieved to disk.

2.1.5 The operations

The total allocated beam time was one week. After two days of installation and commissioning stable operation was reached. Data was taken in two different modes:

- HIP rate measurement in single trigger mode with different particles and intensities, 300 MeV/c π^- with low intensity (I≈15 KHz, with pre-filter), medium intensity (I≈30 KHz, with and without pre-filter), high intensity (I≈1.2 MHz, with pre-filter), 300 MeV/c π^+ (I≈25 KHz, with pre-filter, with and without APV25 operated in inverting mode) and 50 MeV kinetic energy proton beam.

- Dead-time measurement in multi-trigger mode with 300 MeV/c π^- (pre-filter and backward veto). Around 175 GB of total data volume has been recorded on disks. The data rates were mainly limited by the writing to disk (≈ 2 MB/s).

2.2 The X5 beam test

To complement and cross check the PSI May 2002 measurements, six modules were exposed, in August 2002, to the CERN SPS X5 beam. The setup was basically the same as used in PSI and in the following section it will only be described the slight differences and the main new features with respect to the previous test.

2.3 The X5 beam

The X5 beam was used at 100 GeV/c momentum. The total maximum intensity (10^6 π^- per cycle) was delivered in a 4.8 s spill during a total cycle of 16.8 s over a beam spot of about 1 cm^2. The instantaneous local rate could thus be estimated to be around 2 $\mathrm{KHz/mm}^2$, comparable to LHC conditions. However due to the poor duty cycle imposed by the 16.8 s SPS cycle and the small surface area hit, the integrated HIP production was much lower than in PSI test.

2.4 The experimental setup

The six modules exposed were exclusively recently built TOB type modules with nominal $100\ \Omega$ R_{inv} resistors, except for the second and fourth module downstream of the beam equipped with $50\ \Omega$ resistors. The fifth module rapidly gave trouble so was taken out of the data acquisition and is not used in the analysis. The interface and copper cable to the local PC based ADC were replaced by an analog optical link driving the analog APV information to a distant PC-based ADC in the counting room, as foreseen for the final CMS Tracker operation. In addition to improving accessibility to the equipment, this led to improved common mode noise behavior. In front of the setup, a structure with TEC modules was tested during this data taking, thus contributing additional material on the beam line.

2.5 The trigger

The trigger hardware architecture of the test in X5 was improved with respect to the PSI one:

- Since no synchronization of clocks was needed, the standard TSC card could be used, allowing the refined delay tunings needed for APV deconvolution mode.
- A new VME trigger card was developed, interfaced with the standard LHC trigger system. It implements both the TSC fine-tuning functionalities and the possibility to send bunch trains of triggers for dead-time studies.

The trigger for beam particles was derived from a small 5 x 10 cm^2 scintillation counter for pions runs and 10 x 10 cm^2 counter for muon runs.

2.6 The control and data acquisition

The data acquisition was also improved and implemented the standard Event Builder designed by the XDAQ group. It improved the network usage and permitted to nearly saturate the bandwidth of the fast Ethernet (9 MB/s achieved). The control and monitoring were similar to the ones used in PSI.

2.7 The operations

During a ten day period, various configurations were set up and large quantities of data were recorded. Significant statistics were taken both in APV peak and deconvolution modes. Some additional running time was devoted to measurements with the APV inverter stage disabled to study the effect of this.

3 HIP rate measurements

HIP events are identified on the basis of the effects they cause on the baseline of the APV readout chip. Depending on the energy released in the sensor, a full range of baseline shifts may be induced by HIP events. Integral HIP rate curves are obtained by counting the rate of events where the baseline is shifted by more than a certain threshold. As will be shown in Sections 4 and 5, any perturbation of the baseline can influence the behavior of the APV, causing both inefficiency and spurious clusters.

Two independent analyses are performed, named in the following TT6 and R2, which mainly differ in the way the baseline perturbation is measured. In the TT6 approach the absolute shift of the common mode value is computed: this is expected to be directly related to the energy released in the modules. Integral HIP rate curves are defined, for each module, as a function of the threshold $\mathrm{CM_{cut}}$ imposed on the common mode value. In the R2 analysis the common mode shifts are normalized, for each APV, to the available range, determined by the difference between the average pedestal value and the APV digital zero. For this purpose, the $\mathrm{CM_{RATIO}}$ variable is defined as follows:

$$\mathrm{CM_{RATIO}} = \frac{|\mathrm{CM}|}{(\overline{\mathrm{ped}} - \mathrm{d_0})}$$

where $\overline{\mathrm{ped}}$ is the average pedestal value of all channels in the APV and $\mathrm{d_0}$ is the APV digital zero level in ADC counts. The $\mathrm{CM_{RATIO}}$ variable assesses how close the APV chip is driven to the saturation of the available range, treating all APVs in a consistent way, with no cut tuning APV per APV. In both analyses the CM is computed using the median algorithm.

The two analyses can cross-check each other since they implement independent raw data processing algorithms for pedestal and noise evaluation, common mode noise subtraction and clusterization. These algorithms are developed based on the *ApvAnalysis* package [3], which ensures a well-defined interface to the data acquisition chain and to the standard CMS reconstruction software, ORCA [4].

Figure 2 shows a typical CM distribution obtained for one APV. Ordinary events peak at $\mathrm{CM} \sim 0$, whereas HIP events form the negative tail. HIP events above a given energy release produce the peak at $\mathrm{CM} \sim \mathrm{T^0_{ped}}$, where $\mathrm{T^0_{ped}} = \mathrm{d_0} - \overline{\mathrm{ped}}$ is the low end of the APV output range.

Figure 3 shows in more detail the saturation occurring at $\mathrm{CM} \sim \mathrm{T^0_{ped}}$; the RMS of the truncated distribution of raw ADC values of one APV is plotted versus the CM value. The lower 6 ADC values and the upper 32 ones are excluded from the computation, in order to avoid dead strips and the signal. For ordinary events the RMS reflects both the noise and the spread in the APV pedestals; it lies between 1.5 and 3 ADC counts. For HIP events the RMS reflects a non-flatness induced in the APV baseline, so that larger RMS values often occur when the CM shift is bigger. Finally, when the CM approaches the $\mathrm{T^0_{ped}}$ value, all channels saturate at the APV digital 0 level, resulting in a flat APV baseline and $\mathrm{RMS} < 1$.

The HIP rate of each module is measured, as a function of the induced baseline, by the ratio:

$$\mathrm{Rate(b_{cut})} = \frac{\mathrm{N_{HIP}(b_{cut})}}{\mathrm{N_{track}}}$$

where $\mathrm{N_{track}}$ is the number of incident tracks on each module, $\mathrm{b_{cut}}$ is the baseline shift ($\mathrm{b_{cut}} = \mathrm{CM_{cut}}$ in the case of the TT6 analysis and $\mathrm{b_{cut}} = \mathrm{CM_{RATIO}}$ in the case of the R2 analysis) and

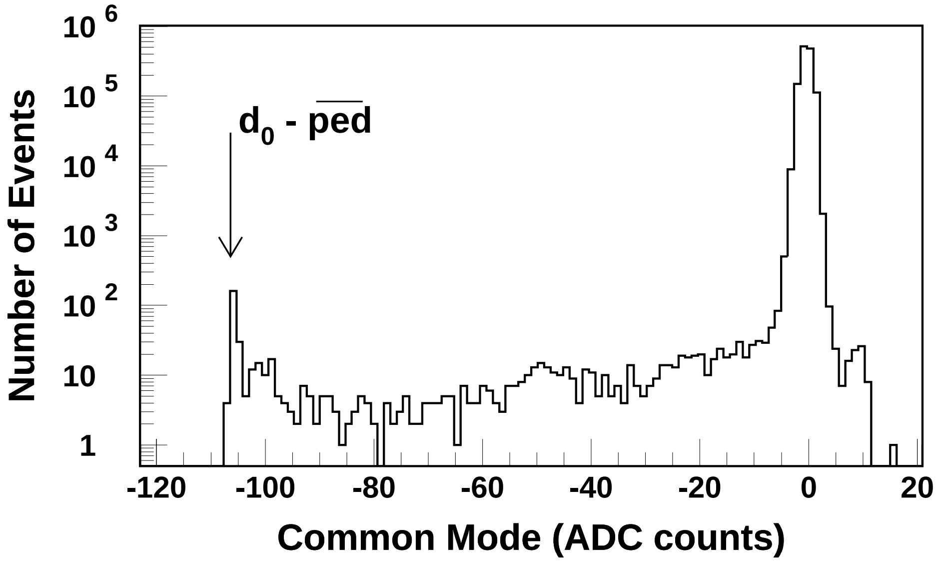

Figure 2: *Common mode distribution for one APV of a TOB module, obtained in the "low-intensity" π^- test at PSI. The arrow points to the* $\mathrm{T}^0_{\mathrm{ped}}$ *value for this APV (see text). The common mode distribution saturates in the neighborhood of* $\mathrm{T}^0_{\mathrm{ped}}$.

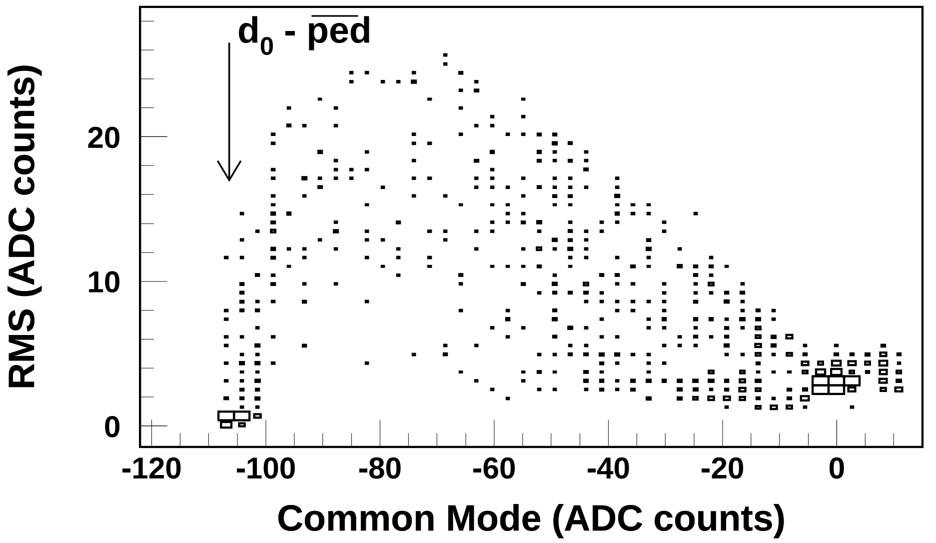

Figure 3: *The RMS of the truncated distribution of raw ADC values versus the common mode for one APV of a TOB module, obtained in the "low-intensity"* π^- *test at PSI. The arrow points to the* $\mathrm{T}^0_{\mathrm{ped}}$ *value.*

N_{HIP} is the total number of HIP candidate events affecting the module and causing the baseline of one APV to be lower than b_{cut}. Integral HIP rate curves are obtained by varying b_{cut}. Events where the APV is still recovering from a previous HIP are excluded by requiring the presence of a large signal due to a HIP: in the TT6 analysis the sum S_4 of the four highest strips in the APV, after common mode subtraction, is required to be higher than 100 ADC counts; in the R2 analysis S, the sum of cluster charges reconstructed in the APV, is required to exceed 100 ADC counts.

The number of incident tracks on each module is computed from the product $N_{track} = N_{trig}^{tot} \times M_{clust}$ of the total number of triggers examined N_{trig}^{tot} and the average multiplicity M_{clust} of clusters per event in the module. The multiplicity is observed to depend on the beam settings and on the trigger conditions. The purpose of M_{clust} is to correct the number of particles per event in the incoming beam; events containing secondary particles (such as δ rays, HIPs, back-scattered pions) or fake clusters (as explained in Sect. 4) do not enter in its computation. In the R2 analysis HIP events and M_{clust} are analyzed on the same event sample, which is pre-selected requiring non-empty triggers containing no more than 20 clusters reconstructed in any module. It is checked that the applied pre-selection does not bias the HIP rate measurement by excluding good HIP candidates. In the TT6 analysis M_{clust} is measured on a sub-sample of the events (including empty triggers), selected by making loose requirements on the maximum difference between the number of clusters reconstructed in different detector planes and the maximum allowed cluster width and charge. These requirements affect M_{clust} by an amount ranging between $5\,\%$ and $10\,\%$, depending on the beam conditions. The evaluations of M_{clust} between the two analyses are always found to agree within $10\,\%$ (see Table 1).

3.1 HIP rates with 300 MeV/c pions

Table 1 summarizes the data taken during the PSI test and used in the HIP rate measurement. In the fourth column is reported the average M_{clust} value measured. Four run categories may be distinguished: “low-intensity” runs taken with a π^- beam, where several of the acquired triggers are actually empty and result in an average cluster multiplicity less than 1; “high-intensity” π^- runs, where on average 1.5 pion tracks traverse the detector for each good trigger; and runs with a π^+ beam, taken either with the APV inverter enabled or disabled.

In low-intensity triggers the tracks pass only through the two central APVs of each module, covered by the scintillator used for the trigger. In triggers from high-intensity runs extra tracks are often present, in addition to the one causing the trigger, and they pass sometimes through the outermost APVs of each module. The four different categories of runs also differ in the applied APV settings, in particular the VPSP parameter affecting the value of T_{ped}^0 [5]. The consistency of HIP rates measured in different run conditions is therefore a useful check on systematic effects.

The relative difference of the M_{clust} value between upstream and downstream modules ranges from $5\,\%$ in “low-intensity” π^- runs up to $10\,\%$ in “high-intensity” π^- runs; it is due to back-scattered pions, which tend to illuminate more the downstream region. Overall, a systematic uncertainty of $\pm 10\,\%$ is estimated on the determination of N_{track}.

Figures 4 and 5 show the integral HIP rate curves measured in high-intensity π^- runs with the TT6 and the R2 analyses as a function, respectively, of CM_{cut} and CM_{RATIO}. Table 2 details the HIP rates for $CM_{cut} = -40$, $CM_{cut} = -90$ ADC counts and for $CM_{RATIO} = -0.8$. The

Table 1: *Data from the PSI test with 300 MeV/c pions analyzed in the HIP rate study.*

	APV configuration	N Events (thousands)	$\mathrm{M_{clust}}$
"low-intensity" π^-	peak, Inv ON	1 285	0.67
"high-intensity" π^-	peak, Inv ON	347	1.48
π^+ Inv. ON	peak, Inv ON	868	1.00
π^+ Inv. OFF	peak, Inv OFF	170	1.00

$\mathrm{CM_{cut}}$ and $\mathrm{CM_{RATIO}}$ values in the table are chosen just as a reference. When measurements from different modules belonging to the same detector category are available, the mean value is quoted. The error on the mean is less than $15\,\%$.

Table 2: *HIP rates per incident pion measured in "high-intensity" π^- runs at* $\mathrm{CM_{cut}}$ *= -40 ADC counts,* $\mathrm{CM_{cut}}$ *= -90 ADC counts and* $\mathrm{CM_{RATIO}}$ *= -0.8 for each category of detector. The errors reported are statistical.*

	Integral HIP rate per incident pion (10^{-4})		
detector	$\mathrm{CM_{cut}}$ = -40 ADC counts	$\mathrm{CM_{cut}}$ = -90 ADC counts	$\mathrm{CM_{RATIO}}$ = -0.8
TIB 50 Ω	5.96 ± 0.36	2.53 ± 0.23	1.71 ± 0.28
TIB 100 Ω	9.60 ± 0.47	5.64 ± 0.36	6.23 ± 0.55
TEC 100 Ω	17.34 ± 0.32	9.86 ± 0.30	10.42 ± 0.36
TOB 50 Ω	15.32 ± 0.31	7.93 ± 0.22	6.36 ± 0.28
TOB 75 Ω	19.57 ± 0.60	10.50 ± 0.44	10.80 ± 0.63
TOB 100 Ω	18.24 ± 0.42	9.78 ± 0.30	8.19 ± 0.39

The $\mathrm{T^0_{ped}}$ values range from 60 to 130 ADC counts (with an average of 115), so that the rates at $\mathrm{CM_{cut}}$ = -90 reported in the table may be approximatively compared to those at $\mathrm{CM_{RATIO}}$ = -0.8. The rates measured with the two analyses agree within $10\,\%$, when both are expressed in terms of $\mathrm{CM_{RATIO}}$.

The thickness of TIB modules is only 320 μm, compared to 500 μm for the TOB modules, and their HIP rates scale accordingly, because of the reduced probability for the occurrence of nuclear interactions and because of the reduced ionization path available to the debris.

The main systematic uncertainties affecting the measured rates derive from the determination of $\mathrm{N_{track}}$ ($\pm 10\,\%$, as explained above) and from the choice of the minimum signal required to identify HIP events. Due to the 16×20 ns event pre-filter imposed at the trigger level, events where the APV is still recovering from a previous HIP event are suppressed. For example varying the requirement on $\mathrm{S_4}$ between 40 and 200 ADC counts, in the TT6 analysis, changes the HIP rate by less than $3\,\%$ at $\mathrm{CM_{cut}}$ = -90 ADC counts. Overall, a systematic uncertainty of $\pm 11\,\%$ is estimated.

The consistency of HIP rates measured with different beam conditions and APV settings is a general test of the systematic uncertainties and of the reproducibility of the measurements. For example, Fig. 6 shows in detail the HIP rates obtained with the TT6 analysis for the second and the third TIB modules (ordered downstream) in various runs. Figure 7 shows the average HIP rates measured on TEC and on TOB modules equipped with $\mathrm{R_{inv}} = 50\,\Omega$ and $\mathrm{R_{inv}} = 100(75)\,\Omega$ inverter resistors. A reasonable consistency between results in different run conditions may be

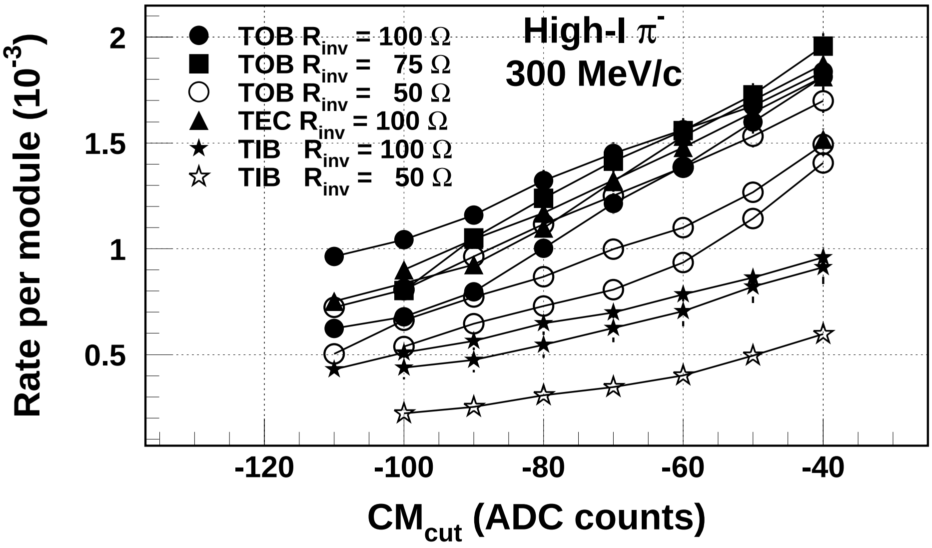

Figure 4: *Integral HIP rate distributions per incident pion from high-intensity* π^- *runs obtained with the TT6 analysis as a function of* $\mathrm{CM_{cut}}$*. The error bars represent statistical errors.*

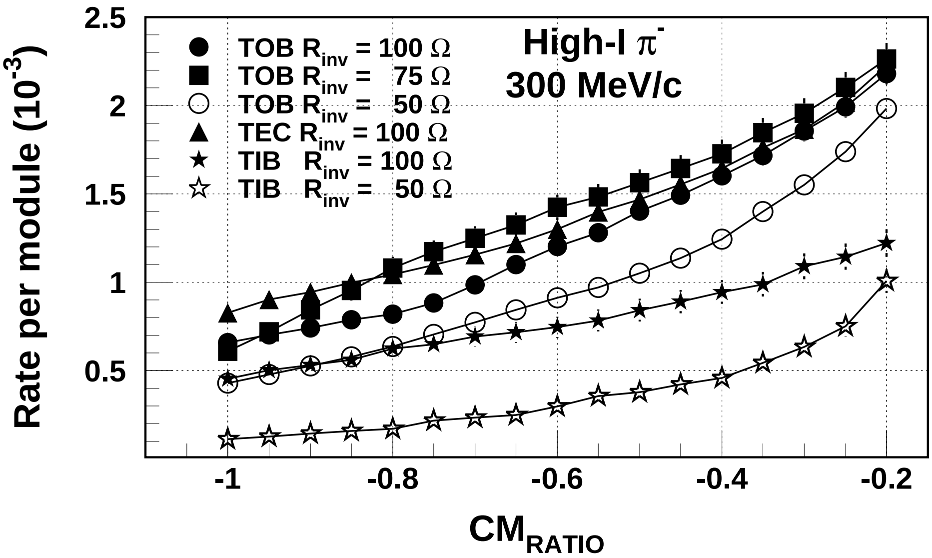

Figure 5: *Integral HIP rate distributions per incident pion from high-intensity* π^- *runs obtained with the R2 analysis as a function of* $\mathrm{CM_{RATIO}}$ *for different detector categories.*

observed: HIP rate curves referring to the same module in different run conditions are parallel, and differ at most by $\pm 25\,\%$.

Data taken with the APV inverter disabled are analyzed by applying a software inversion, replacing the raw ADC values with 512-ADC. In this way negative signals and positive baseline shifts change sign and the standard analysis stream may be followed. The minimum CM value that can be reached is determined by the difference: $\mathrm{T}^1_{\mathrm{ped}} = \overline{\mathrm{ped}} - \mathrm{M}_{\mathrm{sig}}$ where $\mathrm{M}_{\mathrm{sig}}$ is APV dependent and is a few ADC counts higher than the logical digital 1 value. Since, with the standard APV settings, $\mathrm{T}^1_{\mathrm{ped}}$ is usually lower than $\mathrm{T}^0_{\mathrm{ped}}$, larger CM shifts can be studied when the APV inverter is disabled. Within the available CM shift range, the same HIP rates are measured in runs where the APV inverter stage is enabled or disabled.

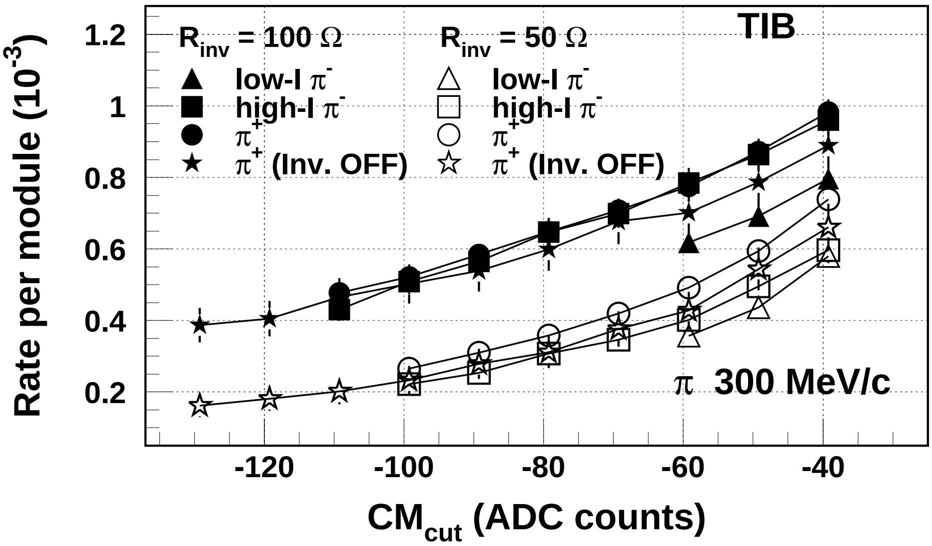

Figure 6: *Integral HIP rate curves per incident pion for the second ($\mathrm{R}_{\mathrm{inv}} = 50\,\Omega$) and the third ($\mathrm{R}_{\mathrm{inv}} = 100\,\Omega$) TIB modules, measured with the TT6 analysis with different beam and APV settings. Error bars represent statistical errors.*

The ratio $\mathrm{R}_{100}/\mathrm{R}_{50}$ between HIP rates measured in modules equipped with $\mathrm{R}_{\mathrm{inv}} = 100\,\Omega$ and $\mathrm{R}_{\mathrm{inv}} = 50\,\Omega$ assesses the difference made by the inverter resistor value in the probability of generating a baseline shift. Based on measurements performed on TOB modules, the ratio $R_{100}/R_{50} = 1.25 \pm 0.25$ is measured, over the full range of accessible common mode shift values. The R_{100}/R_{50} ratio measured for TIB modules is instead $R_{100}/R_{50} = 1.7 \pm 0.3$, based on measurements performed on two modules only. As observed before, HIP rates for detectors of the same kind, equipped with the same value inverter resistor, are the same within $15\,\%$.

The HIP rates measured are inclusive of all effects induced by pion interactions on the twelve detector planes exposed to the beam. These include events where the debris emerging from a nuclear interaction escape the module where they created, generating high energy releases in several modules, and events where non-orthogonal tracks traverse the detectors, due to beam impurities, back scattered pions or interactions in the detector material itself.

Repeating the TT6 analysis with the additional constraint that only the most energetic HIP is counted when multiple HIP candidates occur in the same event, HIP rates at $\mathrm{CM}_{\mathrm{cut}}$ = -40 ADC

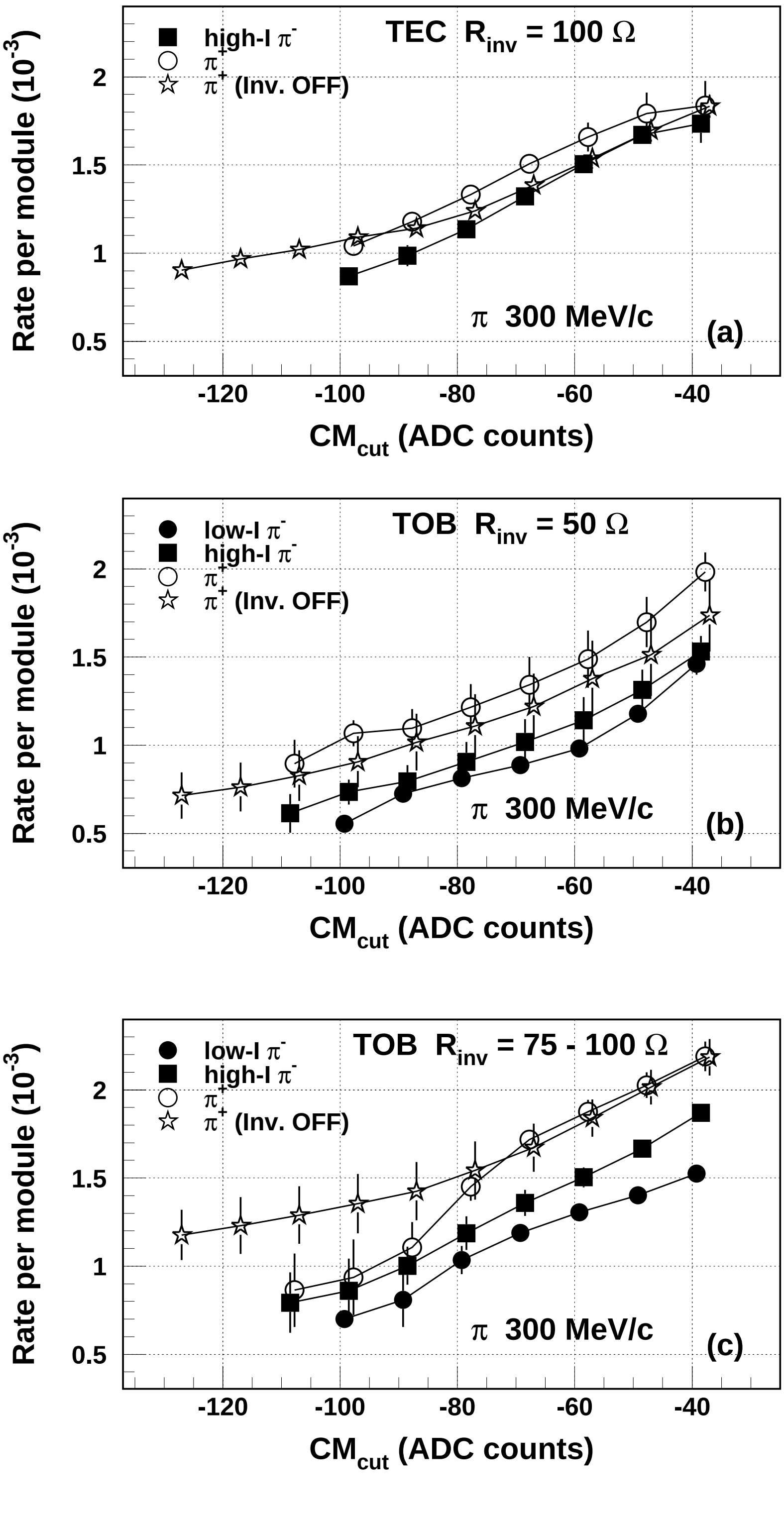

Figure 7: *HIP rate distributions per incident pion measured with the TT6 analysis with different beam and APV settings for (a) TEC modules, (b) TOB modules equipped with* $\mathrm{R_{inv}} = 50\,\Omega$ *and (c) TOB modules equipped with* $\mathrm{R_{inv}} = 100\,\Omega$ *or with* $\mathrm{R_{inv}} = 75\,\Omega$. *The mean value for each group of three modules is displayed. The error bars represent the errors on the mean. Slight shifts to the* $\mathrm{CM_{cut}}$ *graphical representations are applied, in order to avoid superposition of the error bars.*

counts are reduced by $20\,\%$, while those at $\mathrm{CM_{cut}}$ = -90 ADC counts are reduced by $10\,\%$.

Tracks non-orthogonal to the modules traverse a longer path in the detector material, increasing the probability of generating HIP events. An additional analysis is performed, where HIP candidates in one module are selected only when there is one cluster in each of the two immediate upstream modules, with the track segment defined by the two clusters pointing to the HIP region with an angular coefficient lower than 0.3. Events with multiple HIP candidates are rejected. The rate per module measured in this way is $20\,\% - 40\,\%$ lower with respect to the one measured with the TT6 analysis, depending on the $\mathrm{CM_{cut}}$ value.

3.2 HIP rates with 120 GeV/c pions

Table 3 summarizes the data analyzed during the X5 test and used in the HIP rate measurement. Three types of run may be distinguished: deconvolution mode, both with the APV inverter stage enabled and disabled, and peak mode with the APV inverter stage disabled.

Table 3: *Data from the X5 test with 120 GeV pions analyzed in the HIP rate study.*

APV configuration	N Events	$\mathrm{M_{clust}}$
deconv., Inv ON	258 k	2.27
deconv., Inv OFF	197 k	2.35
peak, Inv OFF	93 k	2.59

HIP rates measured using the TT6 and the R2 analyses in deconvolution mode, with the APV inverter enabled, are detailed in table 4. Figure 8 shows the integral HIP rate curves obtained with the R2 analysis.

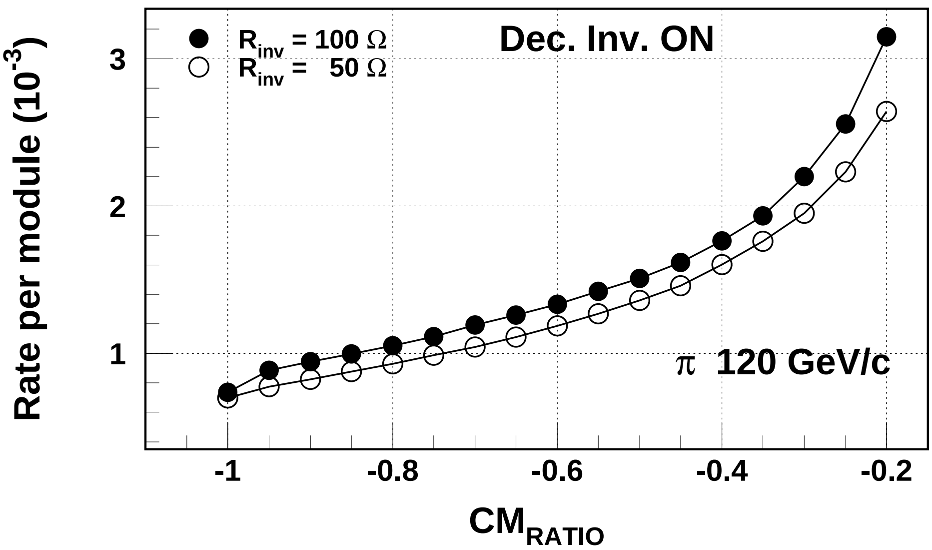

Figure 8: *HIP rates per incident pion measured by R2 analysis for TOB detectors with 120 GeV/c pions.*

The rates measured with 120 GeV/c pions are similar to those measured at PSI with 300 MeV/c

Table 4: *HIP rates per incident pion measured with 120 GeV pions in runs taken in deconvolution mode with the APV inverter stage enabled at* $\mathrm{CM_{cut}}$ *= -40 ADC counts,* $\mathrm{CM_{cut}}$ *= 90 ADC counts and* $\mathrm{CM_{RATIO}}$ *= -0.8 for each category of detector. The errors reported are statistical.*

	Integral HIP rate per incident pion (10^{-4})		
detector	$\mathrm{CM_{cut}}$ = -40 ADC counts	$\mathrm{CM_{cut}}$ = -90 ADC counts	$\mathrm{CM_{RATIO}}$ = -0.8
TOB 50 Ω	16.96 ± 0.37	10.66 ± 0.42	9.30 ± 0.27
TOB 100 Ω	14.34 ± 0.34	10.37 ± 0.42	10.51 ± 0.23

pions. Modules equipped with different inverter resistors give the same rates. When both expressed in terms of the $\mathrm{CM_{RATIO}}$ variable, results from the TT6 and R2 analyses are consistent and differ at most by $10\,\%$.

As for PSI measurements, the main systematic uncertainties arise from the determination of $\mathrm{N_{track}}$ and the choice of the minimum signal required to identify HIP events. From the difference of the cluster multiplicity of different detector planes and by varying the pre-selection procedure the uncertainty on $\mathrm{N_{track}}$ is estimated to be $\pm 12\,\%$. Since no trigger pre-filter is present in the X5 test, the contamination due to events where the APV is still recovering from a previous HIP is not negligible. The effect depends on the APV inverter stage configuration, since (as shown in Sect. 4) when the inverter stage is switched OFF a faster APV recovery is expected. In the TT6 analysis, when the cut on $\mathrm{S_4}$ is varied between 40 and 200 ADC counts, a variation of $22\,\%$ of the HIP rate is observed in runs in deconvolution mode with inverter ON, whilst a variation of less than $4\,\%$ is observed in runs with the inverter OFF. By studying the topology and the time evolution of a sample of HIP candidate events taken in deconvolution mode, which were rejected because their APV signal was too small, it is found that several of them are actually inconsistent with APV recoveries after a previous HIP, but they are good HIP events where the signal development is delayed by several tens of nanoseconds. Overall, a systematic uncertainty of $\pm 19\,\%$ on the rates measured in deconvolution mode with inverter ON is estimated.

Figure 9 reports HIP rate curves obtained with the TT6 analysis in the three kinds of run listed in Table 3. Differences in rate between peak and deconvolution modes are less than $20\,\%$. Rates with the inverter stage ON are confirmed to be the same order as rates with inverter stage OFF. The HIP rates measured at $\mathrm{CM_{cut}}$= -140 ADC counts may be compared to those reported in [1], measured in the 2001 X5 beam test. Rates presently measured are twice those reported in [1] (8×10^{-4} against 4×10^{-4}) but still consistent within the uncertainties involved with the two analyses.

When the TT6 analysis is repeated imposing that only the most energetic HIP is counted when multiple HIP candidates are present in same event, HIP rates at $\mathrm{CM_{cut}}$ = -40 ADC counts are reduced by $15\,\%$, whilst HIP rates at $\mathrm{CM_{cut}}$ = -90 ADC counts are reduced by $8\,\%$. Upstream of the TOB modules one TEC petal detector is present, equipped with a thick support plate and aluminum box, for a total aluminum thickness of 12 mm, which in some events acts as a pre-shower, spoiling the purity of the beam traversing TOB modules. When the analysis is repeated, selecting events where only one cluster is found in both the first and the second TOB modules, the HIP rates obtained are $30\,\% \;-\; 40\,\%$ lower, depending on the $\mathrm{CM_{cut}}$ value.

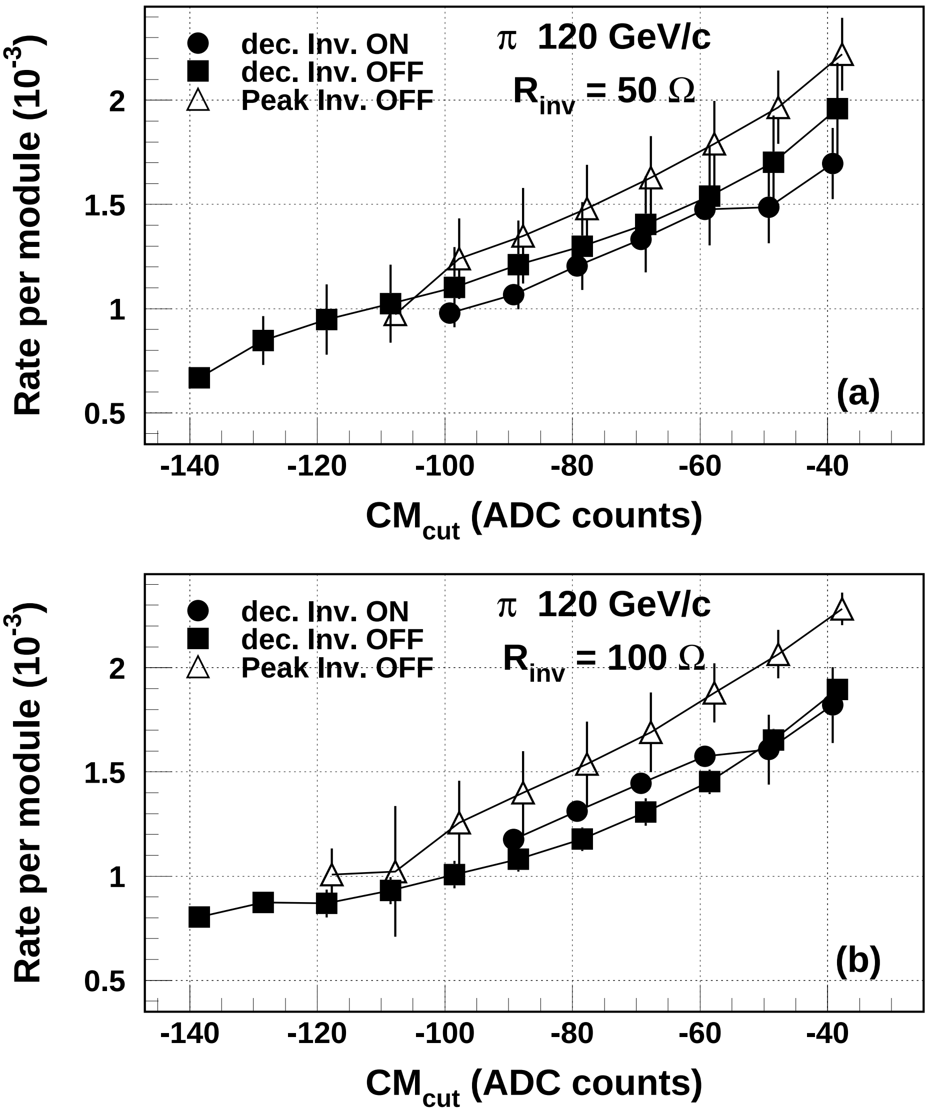

Figure 9: *HIP rate distributions per inciden pion for TOB modules, measured in the X5 beam test, with several APV settings. (a): modules equipped with* $\mathrm{R_{inv}} = 50\,\Omega$*. (b): modules equipped with* $\mathrm{R_{inv}} = 100\,\Omega$*. The average rate for each group of detectors is plotted, while the error bars represent the error on the mean.*

3.3 HIP rate measurements with 50 MeV protons

Data taken during the PSI test with the proton beam of 50 MeV kinetic energy (around 300 MeV/c momentum) are employed to measure the HIP rate. Protons release in the silicon a higher ionisation energy with respect to pions of equal momentum.

Table 5 reports HIP rates measured with the PSI proton beam of $50\ \mathrm{MeV}$ kinetic energy for $\mathrm{CM_{cut}}$ = -40 and $\mathrm{CM_{cut}}$ = -90 ADC counts.

Table 5: *HIP rate results per incident proton measured with 50 MeV kinetic energy protons in the PSI test. Errors are statistical only.*

	Integral HIP rate per incident proton (10^{-4})	
module number	$\mathrm{CM_{cut}}$ = -40 ADC counts	$\mathrm{CM_{cut}}$ = -90 ADC counts
TIB1	12.5 ± 2.3	3.3 ± 1.5
TIB2	5.7 ± 0.9	1.6 ± 0.5
TIB3	13.3 ± 1.4	5.2 ± 0.9
TEC1	41.2 ± 2.4	16.0 ± 1.5
TEC3	38.0 ± 2.3	9.1 ± 1.2

Due to their very low velocity, only few protons are able to reach the second box of modules in time with the sampling time. HIP rates are therefore available only for the first box of detectors. Moreover, due to the adopted APV settings, the TEC2 module has a limited output range $|\mathrm{T^0_{ped}}|$ available to its baseline, so it is not included in the rate computations. Results for the TIB1 module have a higher error, due to the reduced event statistics, since only half of the module was operated.

The beam contamination from pions is lower than $2\,\%$. The systematic uncertainty on the rate measurement is $\pm\,20\,\%$ coming mainly from the determination of $\mathrm{N_{track}}$.

Rates for $\mathrm{CM_{cut}}$ = -90 ADC counts are not dissimilar from those measured with pions; rates for $\mathrm{CM_{cut}}$ = -40 ADC counts are a factor 2 higher, since they are contaminated by the peak at CM $\sim$ -15 ADC counts caused by the proton ionization energy, as explained in the next sub-section.

3.4 Comparison of measured HIP rates with simulations.

In order to compare the measured HIP rates with the integral energy-deposition distributions simulated in Ref. [6], a relation must be established between the observed baseline shift and the energy deposition. The relation between the CM shift and the signal collected by the strips affected by a highly ionising particle is highly non-linear (since the strips quickly saturate) and cannot be used for this purpose. Assuming the relation between the observed baseline shift and the energy released to be linear, data from a few runs taken in the PSI test with a proton beam of $50\ \mathrm{MeV}$ kinetic energy may be used. On traversing 500 μm of silicon, $50\ \mathrm{MeV}$ protons lose on average 1 MeV ($\equiv 6$ MIPs) through ionization. The resulting signal is sufficient to cause an observable shift in the baseline. Figure 10 shows the CM distribution in TEC modules exposed to the proton beam. A clear clustering of events between CM = -10 and CM = -20 ADC counts can be seen. This implies, if one assumes a linear relationship, that the energy deposit required for a baseline shift of -90 ADC counts is between 4 and 9 MeV. This is of the same order of magnitude of the energy estimated in laboratory studies of the HIP effect [2].

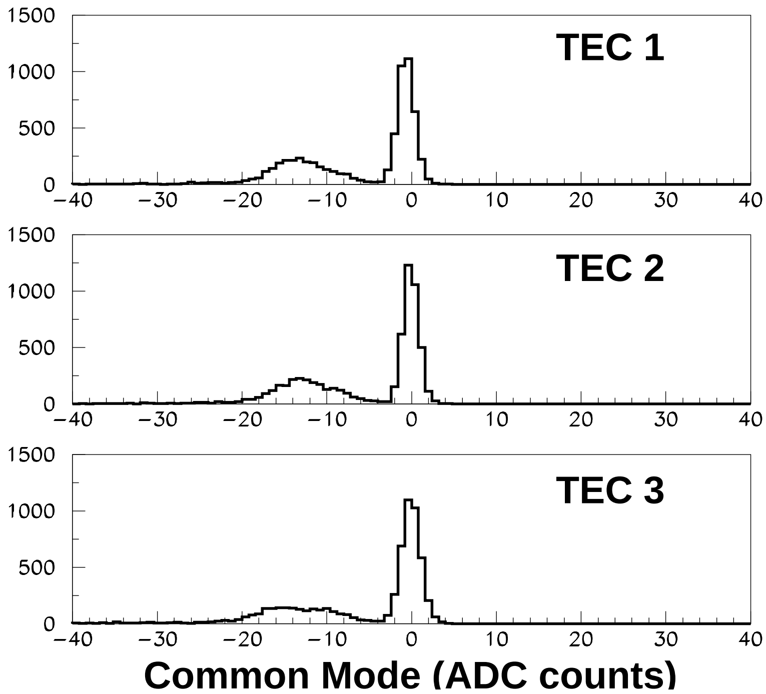

Figure 10: *Common Mode value distribution for the TEC modules in proton runs.*

The HIP rates measured at PSI with the low-energy pion beam and those measured at X5 with the high-energy pion beam agree, to within a factor two, with the rates predicted by the simulation in $4 - 9$ MeV energy deposition range (from Fig. 5 of Ref. [6]). This is good agreement, considering the uncertainties quoted on both the simulation and the measurements.

4 Baseline behaviour following a HIP

Following a HIP, the APV baseline swings low, before slowly recovering to its normal level. This Section is divided into two subsections. The first describes the distortions seen in the shape of the baseline during the recovery, while the second addresses the time required for the recovery.

4.1 Baseline distortions

Test-beam data show that when recovering from a HIP, the common-mode offset in APV chips usually is not flat across the 128 channels. A typical event displaying this problem is shown in Fig. 11. This is potentially a serious problem, since once CMS is running, common-mode subtraction will be performed by the tracker FEDs, as part of their zero suppression algorithm. The algorithm used must be simple in order to fit into the FED's FPGA chips. Currently, it is envisaged that the common-mode offset will be estimated from the median pulse-height on the 128 strips. This implicitly assumes that the common-mode offset is the same for all the strips. Hence non-flat common-mode noise may lead to loss of efficiency for some strips and fake clusters appearing on others. This Section describes the analysis of the problem.

To quantify the non-flatness of the pedestal subtracted baseline, one can calculate the common-mode offset from the median pulse height on each group of 16 strips in an APV, and then plot the rms spread in the 16 common-mode values obtained for each APV. The result obtained with the X5 data is shown in Fig. 12 as a function of event number following a HIP. Note that at X5, events were read out every 75 ns following a HIP.

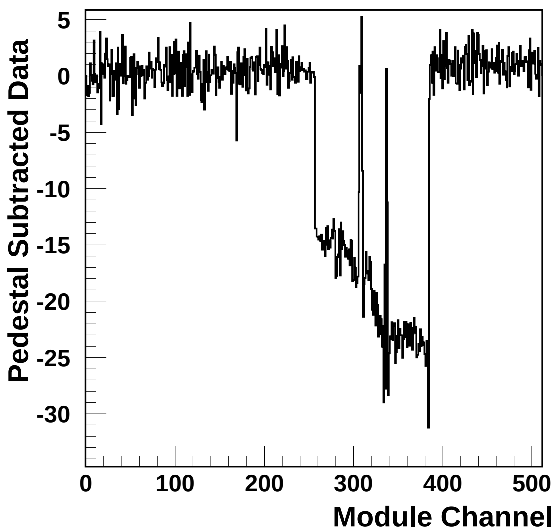

Figure 11: *Example of the pedestal subtracted data in a module affected by a HIP at PSI. The third APV in the module shows significant distortions in the baseline.*

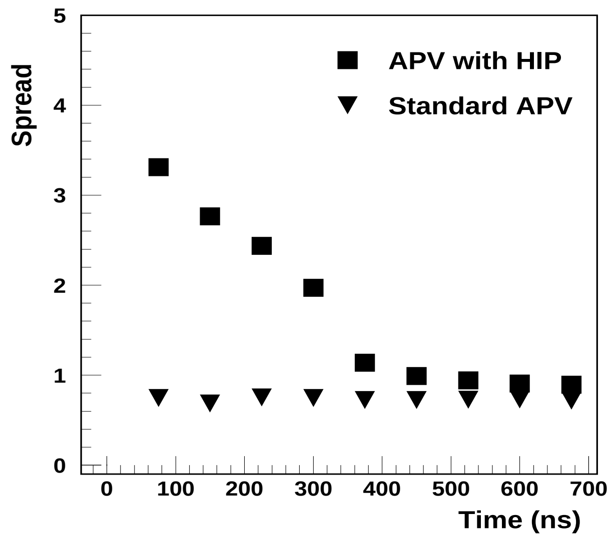

Figure 12: *The rms non-flatness of the baseline (defined in the text) of an APV as a function of event number following a HIP. The data were taken in deconvolution mode at X5, using modules equipped with 50 Ω resistors.*

The TT6 analysis of the number of fake clusters produced by HIPs proceeds as follows. Cluster finding is performed using the algorithm currently being implemented in the FED zero suppression firmware [9]. This selects isolated strips with Signal/Noise $(S/N) > 5$ and non-isolated ones with $S/N > 2$. (N.B. The numerical values of these cuts are programmable and may be retuned when CMS data taking begins). A cluster is defined as a group of strips meeting these criteria. Common-mode subtraction is performed using the standard FED algorithm [9], which estimates the common-mode offset from the median pulse height on the 128 strips of each APV. Nonetheless, to understand if one could benefit by using other algorithms, the analysis is repeated determining the common-mode in smaller groups of strips (64, 32, 16). In addition, the effect of a further zero suppression cut requiring the cluster width to be less than 5, 10 or 15 is tried. Events with HIPs are selected by requiring the common-mode offset to exceed -40 ADC counts.

To remove the effect on the results of genuine clusters, results are based on the difference between the number of clusters (strips) seen in the APV affected by the HIP and the number in the good APV sitting in front of it. These differences are defined as the number of 'fake clusters (strips)'.

Figure 13 shows the mean number of fake clusters and fake strips as a function of time elapsed since the HIP. The plots are based on X5 data taken in APV deconvolution mode with the inverter enabled. Results are given separately for $\mathrm{R_{inv}} = 50$ and 100 Ω and also for common-mode calculations performed in groups of 128 or 16 strips. For the 128 strip common-mode calculation, the results for $\mathrm{R_{inv}} = 50\ \Omega$ show substantially more clusters during the first few hundred nanoseconds (when the baseline is still saturated), and these clusters are significantly wider than for $\mathrm{R_{inv}} = 100\ \Omega$.

To evaluate the consequences of such fake clusters for CMS, two quantities are measured: $N_{cluster} = n_{cluster}/n_{\mathrm{hip}}$ and $N_{strip} = n_{strip}/n_{\mathrm{hip}}$. These are respectively, the average total number of fake clusters and of fake strips produced by a HIP, summed over all the (25 ns) bunch crossings following the HIP. The measured values of these two quantities are given in Table 6, and will be used in Sect. 6.3 to assess if fake clusters significantly affect the data rate expected from the CMS tracker. The results in this table are broken down in several different ways to help understand what influences the fake rate. Namely:

1. APV configuration: peak/deconvolution and inverter stage on/off.
2. Inverter resistor value $\mathrm{R_{inv}}$.
3. Common-mode subtraction and zero suppression algorithms.

A complication is that at the X5 test beam, the data were read out only every 75 ns, as opposed to every 25 ns as at PSI, so three times fewer fake clusters per HIP are seen. Therefore, the total number of fake clusters (strips) seen per HIP at X5 must be multiplied by factor of three to correct for this. This correction is included in Table 6. However, it can only be approximate, as it assumes that the number of fake clusters does not vary on time-scales short compared with 75 ns.

A further concern is that, as shown in Fig 13, the number of fake clusters/strips does not fall to zero by the end of the 30 bunch-crossing observation period. In consequence, the results in Table 6 presumably underestimate the number of fake clusters/strips.

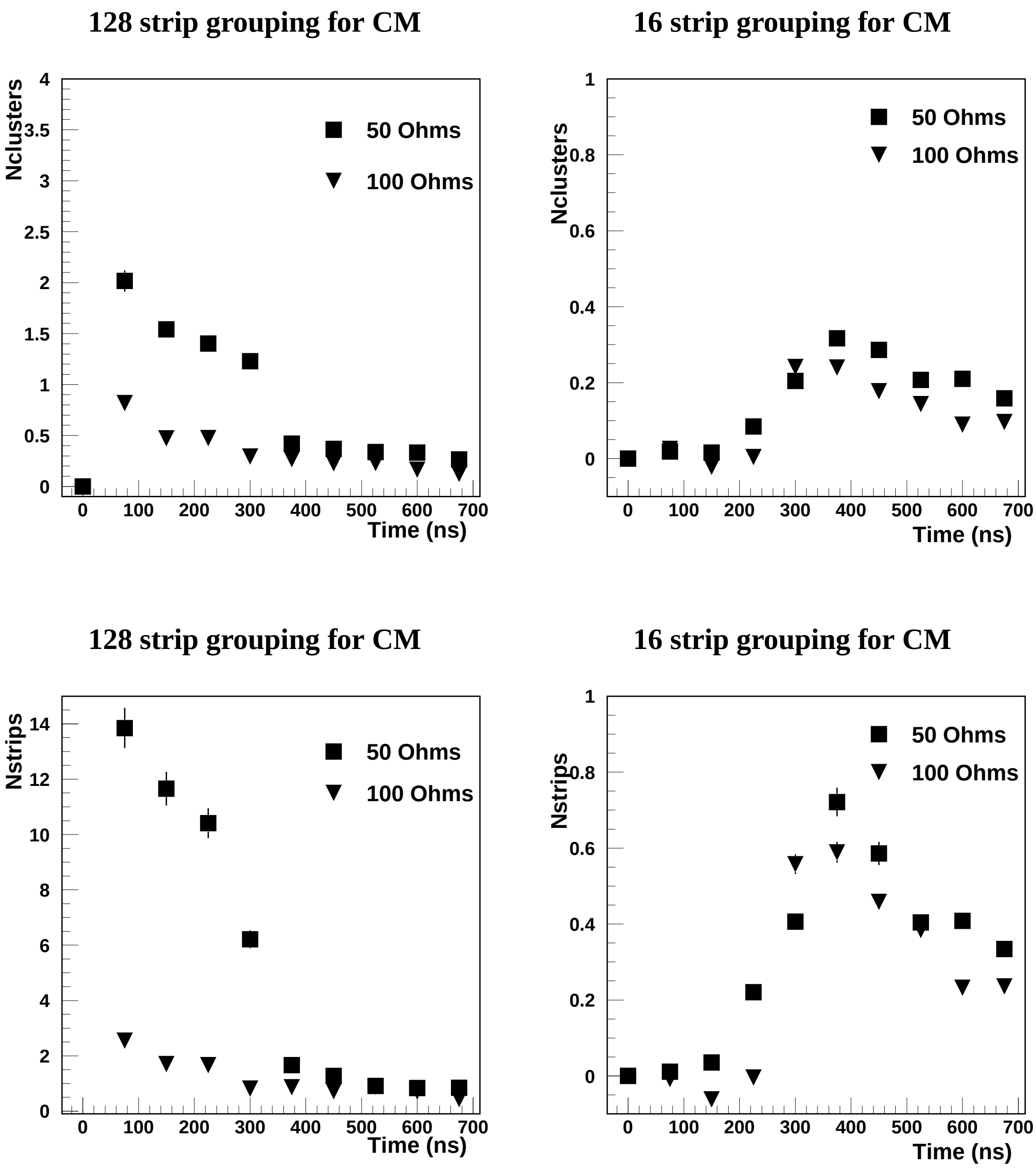

Figure 13: *Mean number of fake clusters (upper plots) and strips (lower plots) as a function of time elapsed since the HIP, for X5 data taken in deconvolution mode with the inverter enabled. Note the different vertical scales.*

Table 6: *The mean number of fake clusters $N_{cluster}$ and fake strips N_{strip} per HIP, summed over all the bunch crossings following each HIP. Results are subdivided according to the APV configuration and according to the value of the resistor $\mathrm{R_{inv}}$. They are also shown for two variants on the standard FED zero suppression algorithm, one of which involves evaluating the common-mode noise for small groups of strips (e.g. $\mathrm{CM}_{nstrips} = 16$), whilst the other involves rejecting all wide clusters (e.g. requiring $\mathrm{W}idth_{clus} < 10$). X5 results have been scaled up by a factor of three.*

Test-Beam	$\mathrm{R_{inv}}$ (Ω)	APV config. Deconv.	APV config. Inv.	Zero Suppression variant	$N_{cluster}$	N_{strip}
X5	50	y	y	standard	24 ± 1	143 ± 8
X5	50	y	y	$\mathrm{CM}_{nstrips} = 16$	4.5 ± 0.3	9.3 ± 0.5
X5	50	y	y	$\mathrm{W}idth_{clus} < 5$	16 ± 1	34 ± 2
X5	50	y	y	$\mathrm{W}idth_{clus} < 10$	19 ± 1	55 ± 3
X5	100	y	y	standard	9.3 ± 0.5	31 ± 2
X5	100	y	y	$\mathrm{CM}_{nstrips} = 16$	3.0 ± 0.2	7.2 ± 0.3
X5	100	y	y	$\mathrm{W}idth_{clus} < 5$	7.0 ± 0.3	15 ± 0.8
X5	100	y	y	$\mathrm{W}idth_{clus} < 10$	9.0 ± 0.5	28 ± 2
X5	50	y	n	standard	25 ± 0.6	54 ± 2
X5	100	y	n	standard	20 ± 0.6	45 ± 1
X5	50	n	n	standard	51 ± 2	262 ± 9
X5	100	n	n	standard	45 ± 2	228 ± 8
PSI	50	n	y	standard	57 ± 2	290 ± 11
PSI	100	n	y	standard	49 ± 2	230 ± 10

4.2 APV baseline recovery

This Section addresses the time evolution of the APV baseline after a HIP event, in the various configurations at PSI and X5. The behavior of the APV baseline is described in terms of the evolution in time of the $\mathrm{CM_{RATIO}}$.

4.2.1 Results in peak mode:

In Figs. 14a–d the evolution of the $\mathrm{CM_{RATIO}}$ of the APVs is shown as a function of time after a HIP event, using the data collected at PSI in peak mode, for TOB modules equipped with 100 and 50 Ω inverter resistors and in the configuration with inverter ON. The HIP events that cause a partially suppressed APV baseline ($\mathrm{CM_{RATIO}} > -0.95$) and a saturated baseline ($\mathrm{CM_{RATIO}} < -0.95$) are collected separately in plots a) and b) for both figures. Two classes of events can be clearly distinguished: in the first are included the events for which the baseline is restored within about 250 ns time, regardless of the $\mathrm{CM_{RATIO}}$ initial value; in the second the baseline starts from a saturated $\mathrm{CM_{RATIO}}$ value, keeps this value for several frames (for ~ 200 ns at most), and finally comes back to its standard value. A fairly long overshoot with respect to the nominal pedestal is also observed in some events.

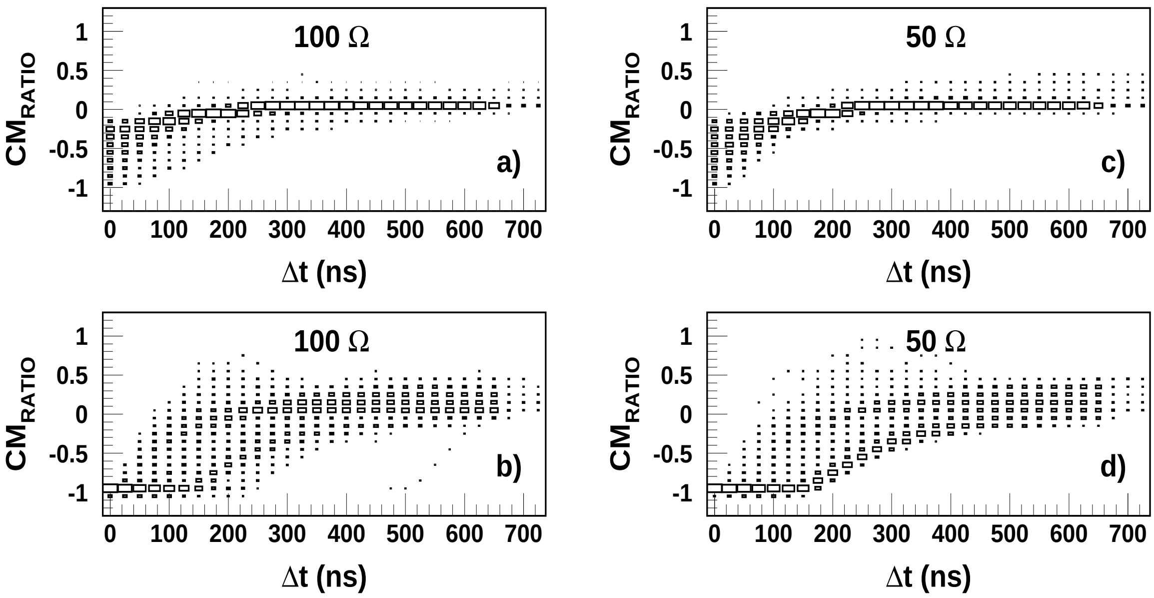

Figure 14: *Baseline recovery of APVs operating in peak mode (PSI data), expressed in terms of* $\mathrm{CM_{RATIO}}$*, for TOB modules equipped with* $\mathrm{R_{inv}} = 100\ \Omega$ *(at left) and* $\mathrm{R_{inv}} = 50\ \Omega$ *(at right), in the confi guration with inverter ON. HIPs are selected with* $\mathrm{CM_{RATIO}} > -0.95$ *in plots (a) and (c), and with* $\mathrm{CM_{RATIO}} < -0.95$ *in plots (b) and (d).*

Figure 15 shows the mean $\mathrm{CM_{RATIO}}$ value as a function of time after a HIP event, for those APVs which initially had $\mathrm{CM_{RATIO}} < -0.95$. Results are shown for various module configurations: TIB, TOB and TEC modules equipped with resistor values $\mathrm{R_{inv}}$ = 50 and 100 Ω. The mean time intervals for which the baseline is recovering (after being saturated in some frames) ($\mathrm{CM_{RATIO}} < 0$) and overshooting ($\mathrm{CM_{RATIO}} > 0$) can be obtained from the curves shown in

Fig. 15.

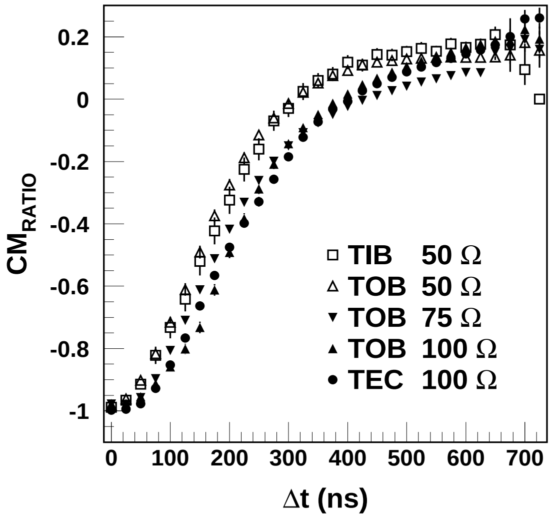

Figure 15: *Mean* $\mathrm{CM}_{\mathrm{ratio}}$ *value as a function of time after a HIP event for various module configurations: TIB, TOB and TEC modules equipped with resistor values* $\mathrm{R}_{\mathrm{inv}} = 50$ *and* $100\ \Omega$*, at PSI.*

4.2.2 Results in deconvolution mode:

The various time evolutions of the APV baseline are also observed in deconvolution mode at X5, as shown in Figs. 16a–d, for TOB modules equipped with 100 and 50 Ω resistors, in the configuration with inverter ON. The recovery of the baseline in deconvolution mode takes longer with respect to peak mode at PSI. The time for which the baseline stays saturated is longer too, as is clear from comparing Fig. 14b/d with Fig. 16b/d. The mean $\mathrm{CM}_{\mathrm{RATIO}}$ value as a function of time after a HIP event is computed for TIB, TOB and TEC modules with resistor values $\mathrm{R}_{\mathrm{inv}} = 50$ and 100 Ω, as shown in Fig. 17.

Both with PSI and X5 data, the reduction of the inverter resistor value from 100 Ω to 50 Ω leads to some reduction in the baseline recovery periods, as can be seen in Figs. 15 and 17.

The fraction of the HIP events in which the baseline is fully saturated is quite APV dependent and can vary a lot according to the APV digital 0 and 1 levels; the mean value of that fraction is about 40 %. The time range in which the baseline is fully saturated could give an indication of the real dead time of the chip.

4.2.3 Results in the configuration with inverter OFF

In Figs. 18 and 19 are reported the evolution of the APV baseline in peak and deconvolution mode respectively, in the configuration with inverter OFF ($\mathrm{R}_{\mathrm{inv}} = 100$ and 50 Ω), based on X5 data. The same two classes of events recognized in Figs. 14 and 16, in which the APV inverter stage is enabled, are visible in Figs. 18 and 19 too. The APV baseline recovery is faster if the inverter is OFF than if it is ON. With the inverter OFF, the recovery takes longer in deconvolution mode than in peak mode.

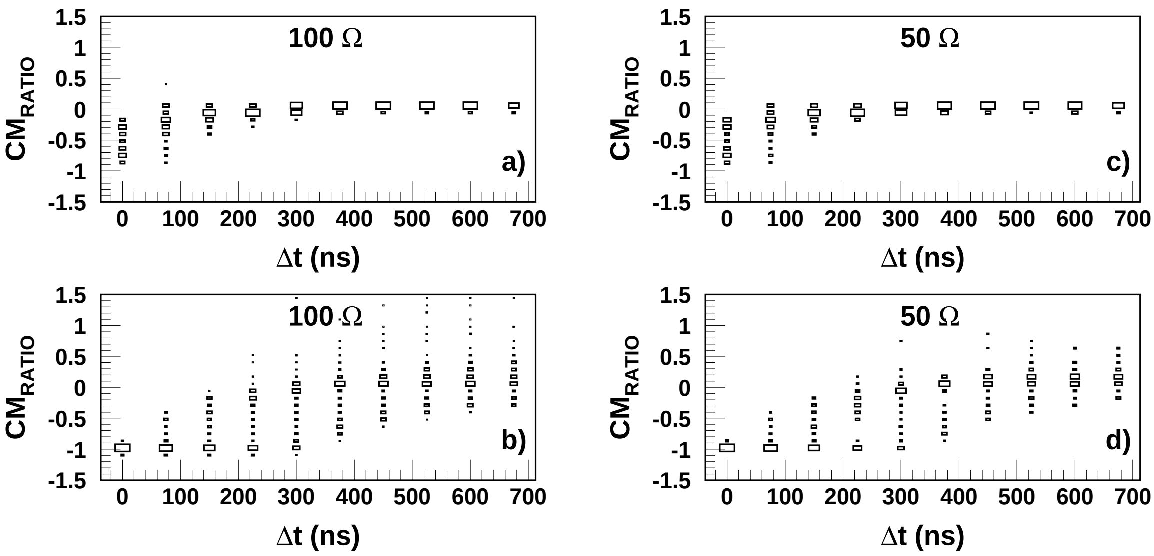

Figure 16: *Baseline recovery of APVs operating in deconvolution mode (X5 data), expressed in terms of* $\mathrm{CM_{RATIO}}$*, as a function of time after a highly ionizing event for TOB modules equipped with* $\mathrm{R_{inv}} = 100\ \Omega$ *(at left) and* $\mathrm{R_{inv}} = 50\ \Omega$ *(at right). HIP events are selected with* $\mathrm{CM_{RATIO}} > -0.95$ *in plots (a) and (c), and* $\mathrm{CM_{RATIO}} < -0.95$ *in plots (b) and (d).*

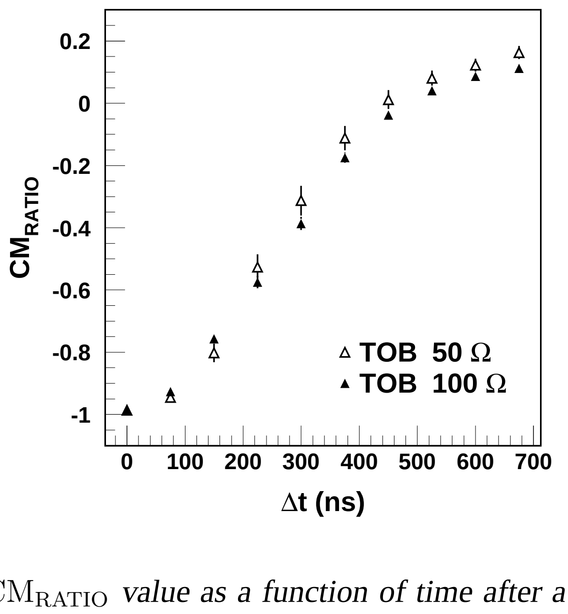

Figure 17: *Mean* $\mathrm{CM_{RATIO}}$ *value as a function of time after a HIP event,for TOB modules equipped with resistor values* $\mathrm{R_{inv}} = 50$ *and* $100\ \Omega$*, at X5.*

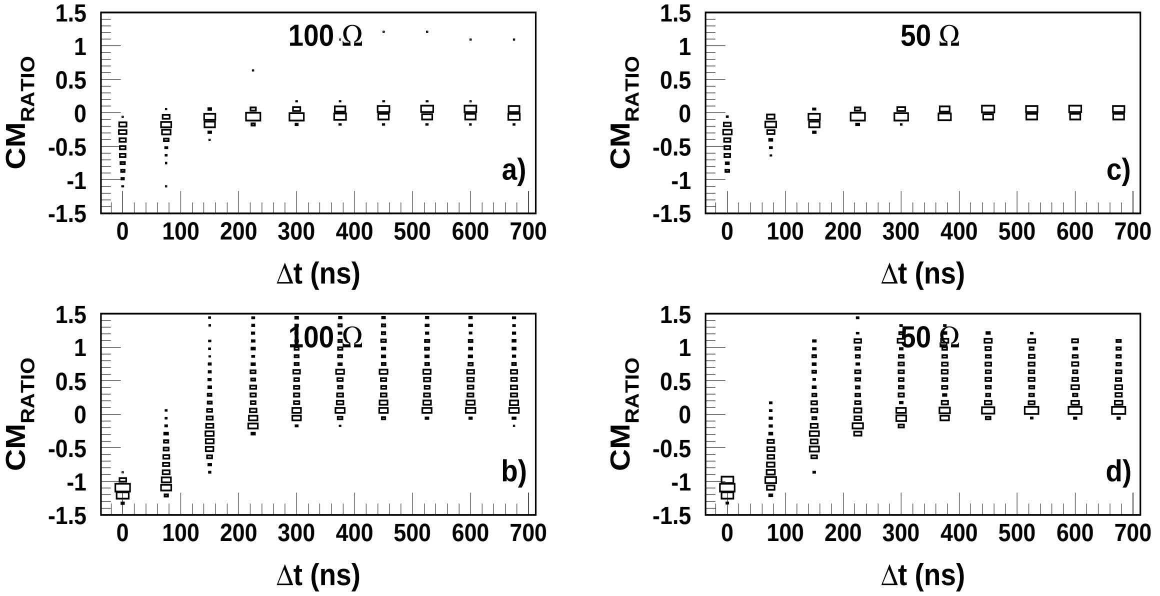

Figure 18: *Baseline recovery of APVs operating in peak mode (X5 data), expressed in terms of* $\mathrm{CM_{RATIO}}$*, for TOB modules equipped with* $\mathrm{R_{inv}} = 100$ *(at left) and* $50\ \Omega$ *(at right), in the configuration with inverter OFF. HIP events are selected with* $\mathrm{CM_{RATIO}} > -0.95$ *in plots (a) and (c), and* $\mathrm{CM_{RATIO}} < -0.95$ *in plots (b) and (d).*

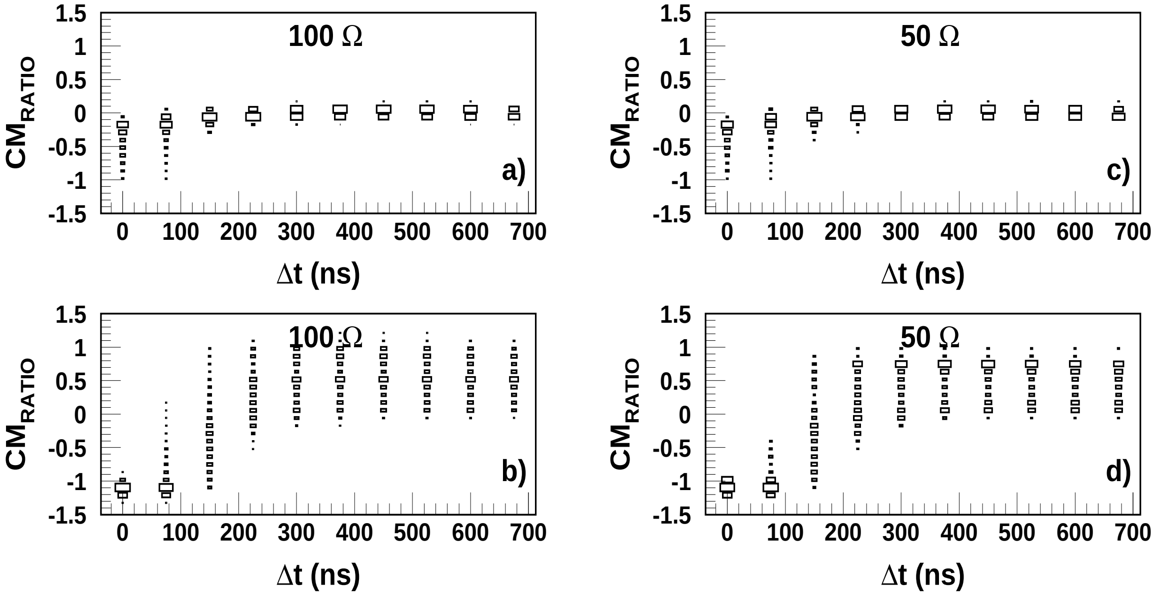

Figure 19: *Baseline recovery of APVs operating in deconvolution mode (X5 data), expressed in terms of* $\mathrm{CM_{RATIO}}$*, for TOB modules equipped with* $\mathrm{R_{inv}} = 100$ *(at left) and* $50\ \Omega$ *(at right), in the configuration with inverter OFF. HIP events are selected with* $\mathrm{CM_{RATIO}} > -0.95$ *in plots (a) and (c), and* $\mathrm{CM_{RATIO}} < -0.95$ *in plots (b) and (d).*

5 APV efficiency measurements

This Section examines how the APV's capability to detect MIP signals recovers following a HIP event. The trains of consecutive events, taken in multi-trigger mode, allow one to follow the time evolution of the APV efficiency for up to 750 ns after a HIP event has occurred. By searching for tracks due to MIP during this period, and checking in which modules they have reconstructed hits associated, one can deduce the APV efficiency.

Only PSI data taken in peak mode are used to extract the results, due to their high statistics of particles traversing the modules. All the results quoted in the following are obtained by selecting the HIP events with the TT6 criteria, as described in Sect. 3, using the cut $\mathrm{CM_{cut}} < -40$ ADC counts. Due to the latency settings of the electronics, the HIPs usually arrived about 100 ns after the start of the 750 ns trigger-train. Therefore this cut is applied not to the common-mode value at time zero, but instead to the minimum common-mode value during the trigger-train.

5.1 The track-finding algorithm

Clusters are searched for in all the silicon modules. The clustering algorithm searches for a seed strip with a signal exceeding 9 ADC counts, then associates neighbouring strips to it if they exceed 8 ADC counts, and finally requires that the total cluster charge exceed 12 ADC counts. (The RMS noise in the TOB modules is ≈ 1.5 ADC counts). The track reconstruction does not use those clusters produced by HIPs or whose width exceeds 9 strips. (The mean width of MIP clusters is 2 strips).

For simplicity, tracking is performed using only the six TOB modules. The track reconstruction algorithm begins from the module having the largest number of clusters, referred to as the seed module. Each cluster in the seed module is considered, in turn, as the seed cluster of a potential track. An exhaustive combinatorial search for clusters in the five other modules is then made, looking in a region where a straight track passing through the seed cluster would lie fully within the acceptance of all the TIB and TOB modules, as shown in Fig. 20a. A least-squares, straight-line fit is performed to all track candidates having at least 5 associated clusters. Where more than one cluster is available in a given module, the cluster which gives the smallest track χ^2 value is used. Tracks with a χ^2 per degree of freedom less than 2 are referred to as good tracks and used in the APV efficiency study.

Due to the poor time resolution of APVs running in peak mode, tracks persist for many consecutive events. The MIP tracks are therefore only selected in the event in which the total charge of the clusters along the track is at its maximum.

The distribution of the difference between the expected and observed positions of hit along a track is shown in Fig. 20b, for each TOB module. The RMS width of the residual distribution is about 2 strips and is largest for the first and the last modules due to the multiple scattering uncertainty.

All the MIP tracks are extrapolated to the module which detected a HIP, intersecting either the APV affected by the HIP or one of the three unaffected APVs. Reconstructed clusters are searched for within 5 strips of the intersection point, with the closest being taken if more than one is found. The charge distributions of these clusters in the module with a HIP are shown in Figs. 21 a and b, for the APVs affected or not by the HIP, respectively. The small bump at low values of charge in Fig. 21 a, is due to a poor estimate of the cluster charge for tracks found in

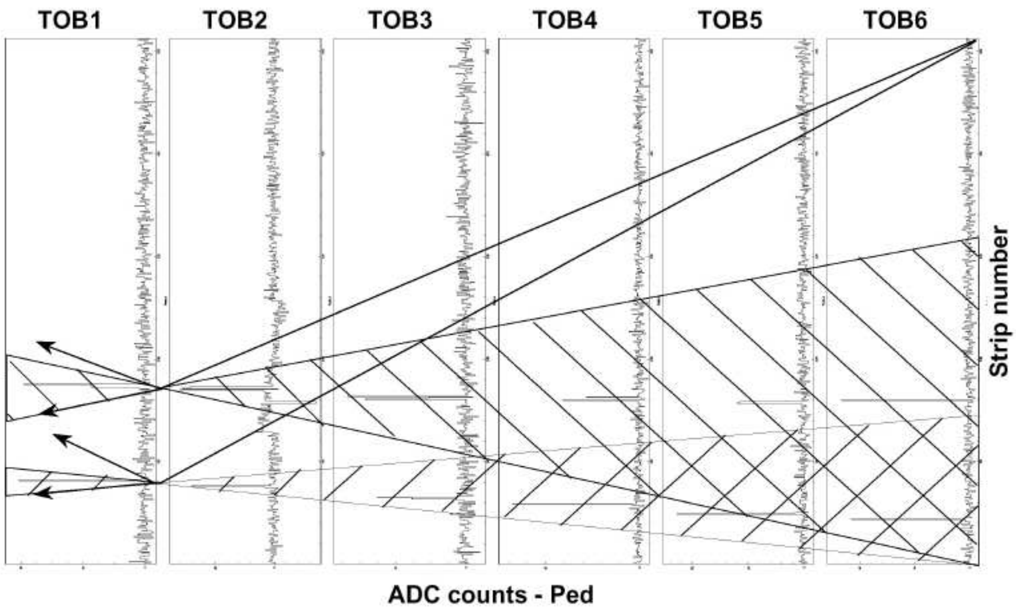

a)

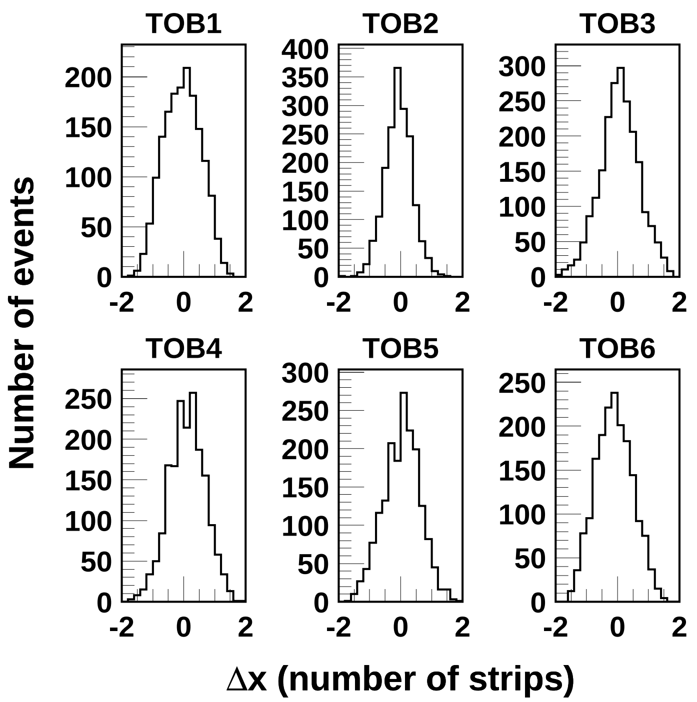

b)

Figure 20: *a) Example of the TT6 track reconstruction algorithm applied to a typical event. For both clusters in the seed module, search regions (hashed) for clusters in other modules are drawn. They encompass the region in which a straight track passing through the seed cluster would lie entirely within the acceptance of all the TIB and TOB modules. b) The difference between the expected and observed positions of clusters associated to tracks, in terms of number of strips, for each TOB module.*

the final few events of the trigger-trains, caused either by overshoot of the APV baseline or by fake clusters located by chance at the expected position of the hit along a track.

The efficiency of the tracking algorithm is about 98%; the residual 2% inefficiency is due to the non-optimal cluster and track-finding algorithms and to the remaining module misalignment.

In order to check the performance of the TT6 track reconstruction, alternative cluster and track-finding algorithms are implemented within the R2 analysis. The R2 procedure to find clusters [9] uses cuts on the signal to noise ratio, $\mathrm{S/N}$, (instead of the signal alone). The $\mathrm{S/N}$ threshold for seed strips is required to be 6, for neighbouring strips is 5 and for cluster as a whole is 8. These thresholds are similar to those used in the TT6 algorithm, given an RMS noise of about 1.5 ADC counts. Clusters are only used by the R2 track reconstruction algorithm if they are less than 5 strips wide.

In each event, the ten clusters with the largest charge, in each module, are considered by the R2 tracking algorithm. Two seed planes are then identified, one from the first three TOB modules and one from the last three TOB modules; both with the most clusters. Modules containing a HIP are discarded. A telescope is defined using one cluster from each of the two seed planes, and all cluster-pair combinations are considered for which the telescope passes through all the modules and has a slope of less than 5 mm/module. A straight-line fit is applied using the nearest cluster in each module within ± 5 strips around the intercept points of the telescope. A track is reconstructed if five clusters are found along the telescope and the fit χ^2 per degree of freedom is less than 2. Tracks are selected only in the event in which the charge of the associated clusters is maximum. The efficiency of the R2 tracking algorithm is similar to the TT6 one.

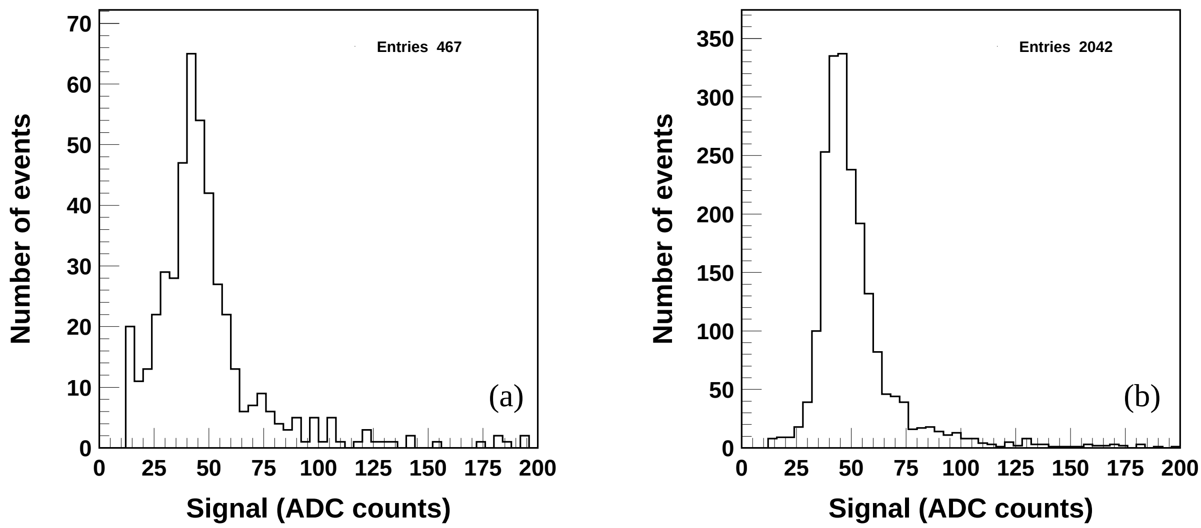

Figure 21: *Signal distribution of MIP clusters, both in: (a) the APV which suffered from a HIP signal, and (b) in those APVs which did not.*

5.2 APV efficiency

The APV efficiency to detect a MIP is defined as the ratio between the number of events in which at least one cluster is found within ± 5 strips around the expected position on a good track and the total number of events with good tracks. The efficiency is computed both for the APVs affected by the HIP and for the others, and studied as a function of the time elapsed since the HIP.

In order to evaluate how the APV efficiency is affected by a HIP signal, it is necessary to correct for other sources of inefficiency, such as those intrinsic to the detector and those due to limitations of the cluster and track-finding algorithms. An unbiased estimate of the efficiency of an APV suffering from a HIP event is obtained dividing that efficiency with the one of APVs not affected by the HIP.

Figure 22a shows that for APVs not affected by a HIP, the efficiency to detect MIP tracks is about the 98%, independent of the time. It also shows that for those events in which the APV baseline is fully saturated by a HIP, the efficiency is close to zero. The efficiency starts to increase as the baseline begins to recover. In APVs affected by HIPs, which do not cause a fully saturated baseline, the average efficiency is initially about 40 %, rising to about 95 % by the end of the trigger-train. The initial value is larger and the recovery time is faster than in the saturated case.

In Fig. 22b, the APV efficiency for modules with different resistor inverter values are distinguished (irrespective of the saturation level of the baseline). The APVs with $\mathrm{R_{inv}} = 50\,\Omega$ have an efficiency of about 20 % larger than those with $\mathrm{R_{inv}} = 100\,\Omega$. After about 500 ns, the efficiency for $\mathrm{R_{inv}} = 50\,\Omega$ APVs reaches 95 % whilst it is only 80 % for $\mathrm{R_{inv}} = 100\,\Omega$ ones.

In Fig. 22c, the global APV efficiency is shown irrespective of the inverter resistor values and of the saturation level of the baseline. The APV efficiency after a HIP event is less than 50 % during the first 100 ns after a HIP.

A common-mode subtraction based on groups of 128 strips is used to derive Figs. 22a–c. However, during APV recovery the baseline is not flat, as described in Sect. 4.1, and a common-mode subtraction based on groups of 16 strips should better take this into account. Figure 22d shows that this does indeed increase the efficiency during the first 200 ns after a HIP, when compare with the results for the 128 strip grouping in Fig. 22c.

Figures 23a and b show the CM values of APVs affected by a HIP, plotted at the time at which a MIP track is identified as passing through the APV. The horizontal axis is the time elapsed between the HIP and the MIP. The two plots distinguish the cases where (a) the APV is efficient, as a cluster associated with the MIP track is found in it, or (b) the APV is inefficient as no cluster is found. Figure 23a shows that for efficient APVs, the CM value recovers in about 250 ns after a HIP. Figure 23b shows that for inefficient, the baseline recovery can take much longer. Furthermore, during the time interval in which the baseline is saturated, the APV is fully inefficient.

The results on the APV efficiency are also derived with R2 analysis for a cross-check. Figure 24a shows the R2 measured APV efficiency as a function of time elapsed since a HIP, in modules equipped with $\mathrm{R_{inv}} = 50$ and $100\ \Omega$. Figure 24b shows the global APV efficiency obtained when doing common-mode subtraction in groups of 128 or 16 strips.

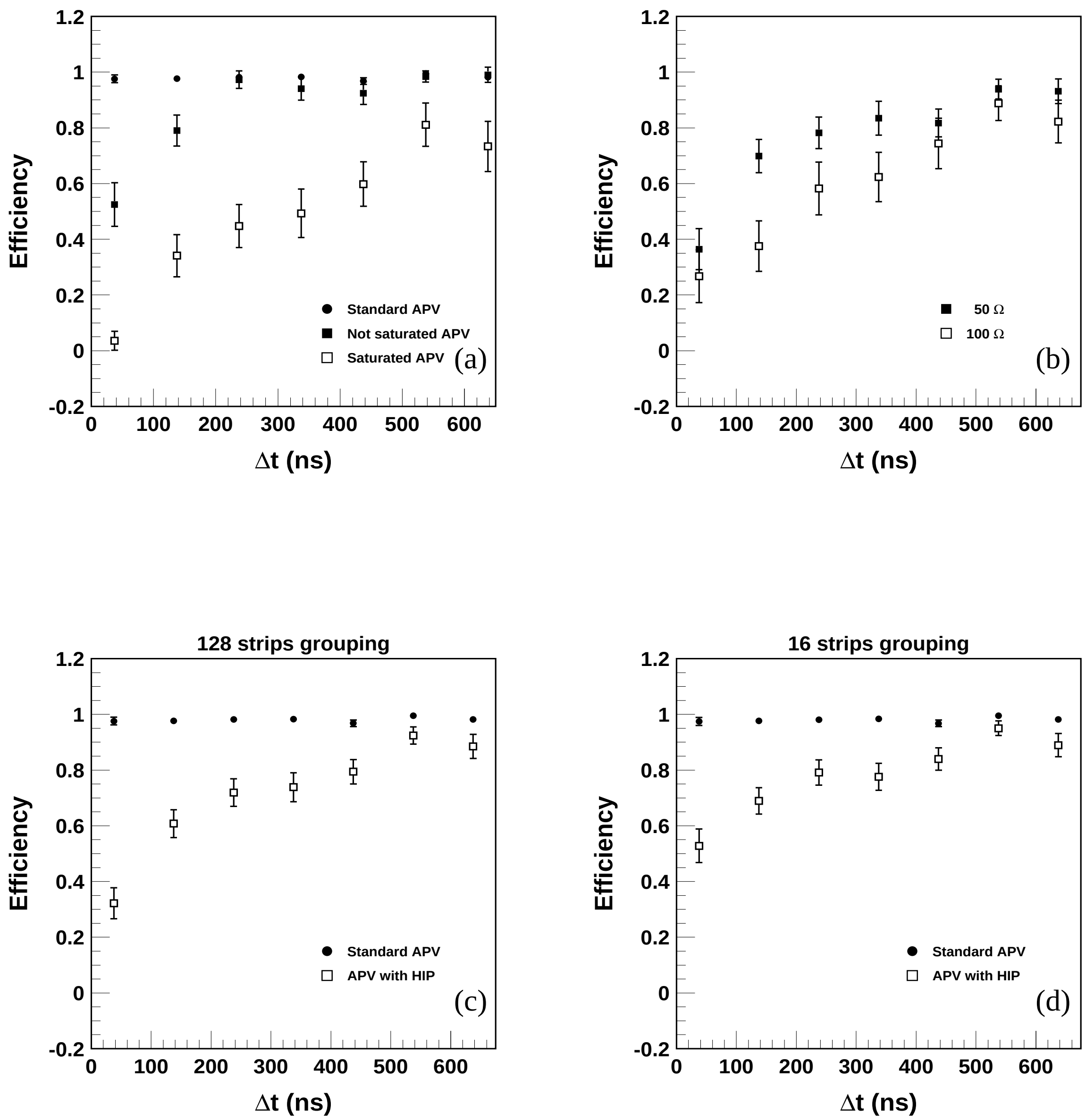

Figure 22: *The efficiency to detect clusters from MIP particles is shown as a function of time elapsed since a HIP: (a) For APVs not suffering from a HIP and for those doing so. In the latter case, the efficiency of APVs where the HIP caused either a full saturation or a partial lowering of the baseline are distinguished; (b) The efficiency of modules equipped with* $\mathrm{R_{inv}} = 50\,\Omega$ *or* $\mathrm{R_{inv}} = 100\,\Omega$ *are distinguished, irrespective of the level of saturation of the APV; (c) Compares the average efficiency in APVs affected or not by a HIP; (d) Similar to the previous plot, but with common-mode subtraction based on groups of 16 strips.*

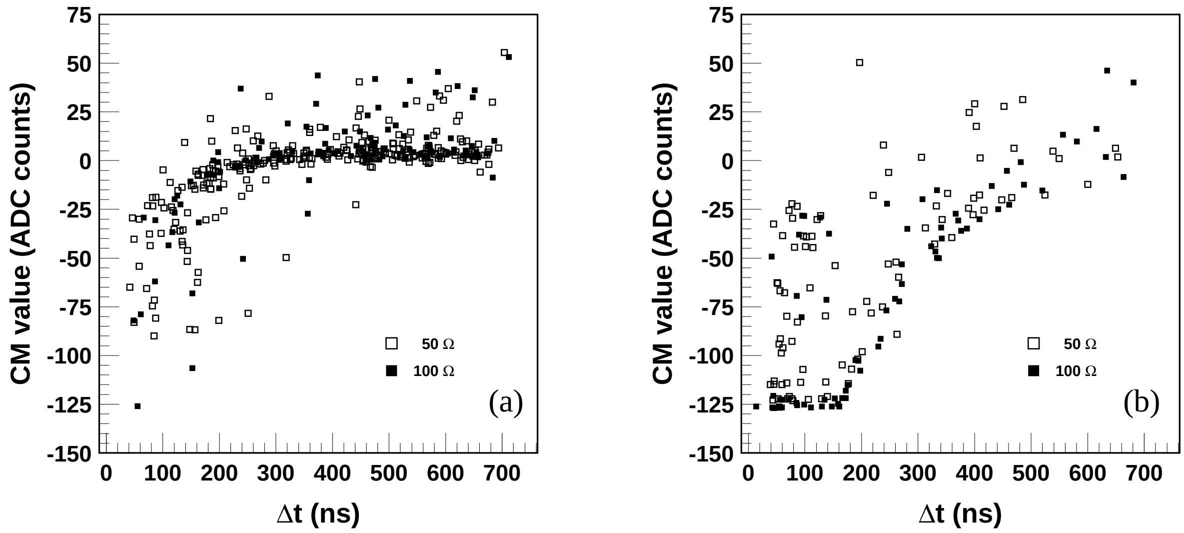

Figure 23: *Evolution of the* CM *as a function of the time elapsed since a HIP, distinguishing the cases when (a) the APV is efficient, or (b) it is inefficient. The contributions from the two inverter resistor values are distinguished.*

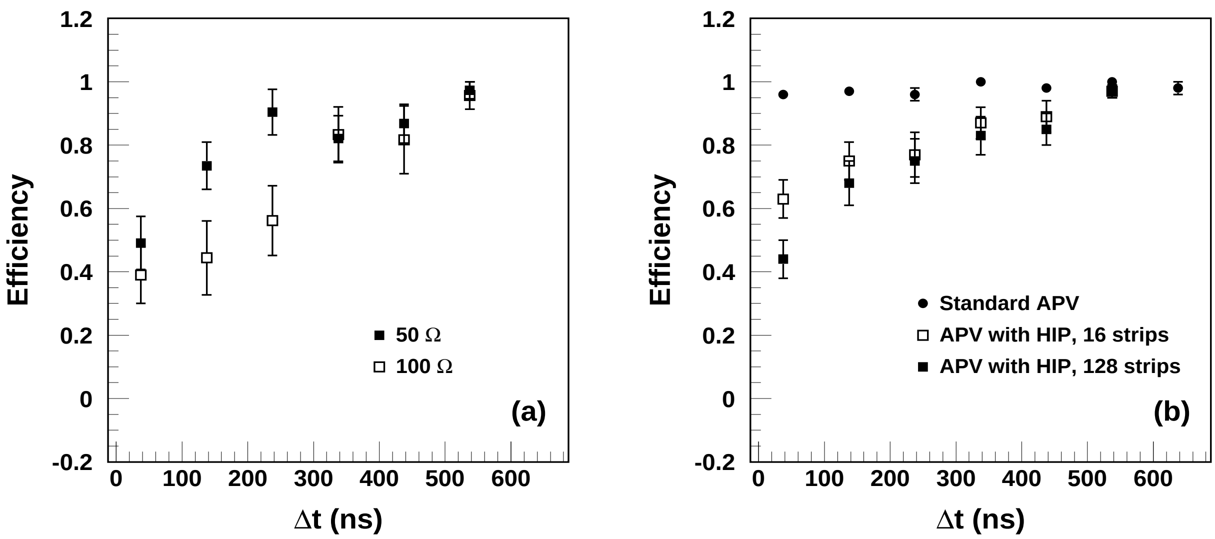

Figure 24: *Time evolution of the APV efficiency from R2 analysis: (a) for modules equipped with* $\mathrm{R_{inv}} = 50$ *and* $100\ \Omega$*; (b) with common-mode subtraction done in groups of 128 or 16 strips.*

The average inefficiency in the 750 ns period after a HIP is computed by averaging the inefficiencies of the successive events in a trigger-train. Figure 25 shows the TT6 mean inefficiency as a function of the HIP selection cut on CM, for two inverter resistor values and two common-mode subtraction strip groupings. These values of the average inefficiency are also listed in Table 7 for two different HIP selection cuts on CM. The APVs equipped with $\mathrm{R_{inv}} = 50\,\Omega$ yield a lower inefficiency with respect to those equipped with $\mathrm{R_{inv}} = 100\,\Omega$.

The mean APV inefficiencies obtained from the R2 analysis are also given in Table 7, where they may be compared with the TT6 results. If common-mode subtraction is done in groups of 128 strips, then the two analyses agree at the level of $\pm$ 10-15 %. This indicates the level of systematic uncertainty related to HIP selection criteria, cluster and track-finding algorithms. The difference is larger when common-mode subtraction is done in groups of 16 strips, indicating increased sensitivity to these systematic effects. The uncertainty related to the finite number of events in each trigger-train (30 at most) cannot be quantified.

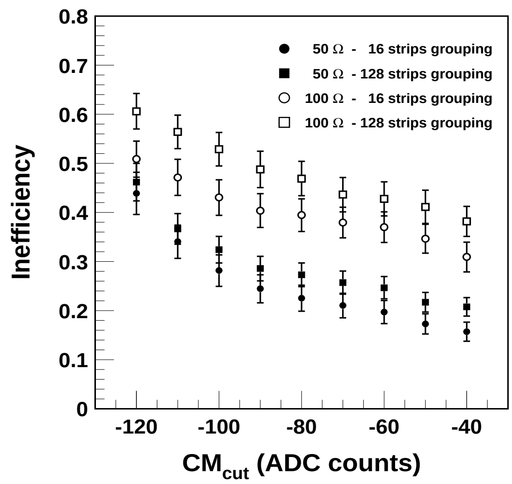

Figure 25: *The TT6 cluster-finding inefficiency averaged over the 750 ns time interval following a HIP, plotted as a function of the HIP selection cut on* CM*, for TOB modules equipped with resistor values* $\mathrm{R_{inv}} = 50$ *or 100* Ω.

6 Expected Effects on the CMS Tracker Performance

In this Section, the effects of HIPs on the CMS Tracker physics performance are evaluated. At LHC energy, each signal event is superimposed over a number of minimum bias events occurring either in the same or in previous/following bunch crossings (respectively called in-time and out-of-time pile-up). These minimum bias events consist mostly of low energy pions, which are confined by the magnetic field to the inner part of the Tracker. In both high and low luminosity data taking, the majority of the interactions between particles and silicon detectors is due to these minimum bias events, and only in the narrow regions inside jets, do the signal events contribute significantly to the hit density.

Table 7: *Percentage average cluster-finding inefficiency over the 750 ns time interval following a HIP. Results are shown for different inverter resistor values, common mode subtraction methods and HIP selection cuts on* CM*. The TT6 and R2 results are compared. The errors reported are statistical.*

		CM subtraction method on a group of strips			
		TT6		R2	
$\mathrm{CM_{cut}}$ (ADC counts)	$\mathrm{R_{inv}}$	128	16	128	16
< -40	50 Ω	21 ± 2	16 ± 2	20 ± 3	11 ± 2
	100 Ω	38 ± 3	33 ± 3	33 ± 4	30 ± 4
< -90	50 Ω	29 ± 3	24 ± 3	27 ± 4	17 ± 3
	100 Ω	48 ± 4	40 ± 3	43 ± 5	38 ± 5

The HIP probability per incident particle is:

$$P_{\mathrm{hip}} = \frac{d}{\lambda} \tag{1}$$

where d is the particle path-length in silicon and λ is an interaction length defined as

$$\frac{1}{\lambda} \equiv \frac{\text{HIP rate}}{\text{module thickness}} .$$

Table 8 shows the results for λ, as obtained by averaging the $\mathrm{CM_{cut}} < -40$ PSI HIP-rate results in Table 2, for modules with 50 Ω or 100 Ω inverter resistors. The errors shown are statistical only. In fact, the individual modules all have $\lambda \approx 30$ cm, with the exception of the 50 Ω TIB module, for which $\lambda \approx 50$ cm. The spread in the value of λ amongst modules of a given resistor value is used to assess the systematic uncertainty on λ. The ratio of the λ value in 50 Ω to 100 Ω λ modules is 1.4 ± 0.4.

According to the results on proton runs, $\mathrm{CM_{cut}} < -40$ corresponds to 2-5 MeV of released energy. As shown in Fig. 6 of Ref. [6], this is the threshold for inelastic nuclear interactions. Therefore λ is expected to be of the order of nuclear interaction length in silicon, i.e. 45 cm at high energies, in good agreement with the results found.

When extrapolating test beam results to the LHC environment, the dependence of λ on the energy spectra and particle type should be taken into account. However as shown in Fig.10 of [6], neglecting the dependence on the particle momentum and type introduces only about 10% additional uncertainty with respect to using the previous test-beam results for 300 MeV/c momentum pions.

More important could be the effects of very low momentum tracks, which can release several MeV by ionization alone, as was observed with the PSI proton beam. The effects of these 'ionization HIPs' are not included in the interaction length λ measured with the PSI pion beam, as its 300 MeV/c momentum was too high to cause such effects. Studies of simulated minimum bias events in the CMS tracker show that only protons will release more than 10 MeV through ionization, with a probability which is about 10 times larger than they have to release this energy through a nuclear interaction. For even lower energy thresholds, the ionization probability would be higher. However, as the energy loss through ionization would then be much softer than that from nuclear interactions (shown in Fig. 6 of Ref. [6]), it is most unlikely that they would

$\mathrm{R_{inv}}$	λ (cm)	$\overline{\eta}$	$\eta_{\rm recovery} \times 10^2$
50 Ω	38 ± 2	0.21 ± 0.02	0.8 ± 0.1
100 Ω	28 ± 1	0.38 ± 0.03	1.9 ± 0.2

Table 8: *Expected $\eta_{\rm recovery}$ in the first TIB layer versus the inverter resistor. The interaction lengths corresponding to the measured HIP rates for $\mathrm{CM_{cut}} < -40$ at PSI are also shown in the second column, while the third column shows, for the same cut, the mean inefficiency in the 30 frames following an HIP. Only statistical errors are shown. For a discussion of the systematics see the text.*

cause comparable APV inefficiency. If the threshold for producing APV inefficiency were as low as 2 MeV then particles other than protons would also need to be considered. Simulation studies show that at high luminosity, about 1.5% of APVs per bunch crossing will collect a charge equivalent exceeding this threshold. If one makes the very pessimistic assumption that each of these 'ionization HIPs' causes half the APV inefficiency of a 'nuclear interaction HIP', then this gives a very conservative limit on possible HIP effects. This hypothesis will sometimes be made below.

The average probability per APV for a HIP to occur in a given LHC bunch-crossing, is related to the mean track-length per APV due to minimum bias event pile-up,

$$\overline{P_{\rm hip}} = \frac{\sum_i w_i \bar{D}_i}{\lambda}\,, \tag{2}$$

where the sum runs over all particle types. The variable w_i is a weight for the i^{th} particle type, corresponding to the probability of it producing any kind of HIP (ionization or nuclear interaction), relative to the probability of it producing a nuclear interaction HIP. The variable $\bar{D}_i$ is the average *total* path length in silicon of all the particles from one bunch-crossing, which traverse the strips read by one APV.

Table 9 shows the value obtained for $w\bar{d}$ in the first and the last barrel layers, as obtained from a simulation of high-luminosity running conditions using CMSIM/ORCA. The results have been cross-checked with those obtained from FLUKA predictions in Table 2 of Ref. [6]. As the FLUKA predictions are found to be lower, results from CMSIM/ORCA are used to be conservative.

6.1 Hit inefficiency

An APV is likely to be completely inefficient in the event where the HIP occurred, i.e. the inefficiency due to HIPs occurring in the present bunch-crossing is:

$$\eta_{\rm hip} = P_{\rm hip}\,.$$

In addition, as shown in Sect. 5, an APV can remain inefficient for several bunch crossings following a HIP. It does however recover almost completely after the 30 bunch-crossing observation period. Therefore the efficiency loss due to the HIPs occurring in previous bunch-crossings can be derived from:

$$\eta_{\rm recovery} = \overline{P_{\rm hip}} \times \sum_{i=1}^{30} \eta_i = 30 \times \overline{P_{\rm hip}} \times \overline{\eta} \tag{3}$$

particle	w	$w\bar{D}$ (μm)	
		first TIB	last TOB
CMSIM/ORCA			
total		480	100
FLUKA			
$\pi^{\pm}$	1	170	15
K$^{\pm}$	1	15	2.5
p	10	170	40
total		355	57.5

Table 9: *Mean weighted track-length per APV per bunch-crossing as obtained from CMSIM/ORCA directly and from FLUKA flux predictions [6]. For results obtained with FLUKA, the breakdown for different particles is also shown.*

where the sum runs over all pertinent bunch crossings prior to the current event. η_i is the measured inefficiency of the i^{th} bunch crossing following a HIP and $\overline{\eta}$ is the average inefficiency in the 30 bunch-crossings following a HIP, as reported in Table 7.

These two effects are combined in

$$\eta_{\rm tot} = 1 - (1 - \eta_{\rm hip})(1 - \eta_{\rm recovery}) \ . \tag{4}$$

In signal events with only a single muon inside the Tracker, hits are lost only due to the pile-up events (i.e., $\eta_{\rm tot} \approx \eta_{\rm recovery}$), since the hit occupancy of the signal event itself is negligible. In Table 8 the expected hit inefficiency in the first TIB layer is shown for two different resistor values. The ratio of 100 Ω to 50 Ω inefficiency is $2.4 \pm 0.4 \pm 0.7$, where the uncertainties are respectively statistical and systematic. The systematic uncertainty is dominated by the uncertainty on the ratio of the interaction lengths.

To study the effect of the 'signal event' component of Eqn. 4, the APV inefficiency due to the HIPs has been implemented in ORCA. In this implementation, for each APV a random number is generated and if its probability is less than $\eta_{\rm tot}$, all the APV's digitizings are deleted and not passed to the reconstruction algorithms. Note that $\eta_{\rm tot}$ will change event by event, because $\eta_{\rm hip}$ depends on the number of tracks passing through each APV in a given event. Table 10 shows the hit inefficiency on signal tracks versus the barrel layer in single muon events and $b\bar{b}$ events with transverse energy $E_T = 100$ GeV for a 50 Ω resistor. The signal track hit inefficiency would approximately double with a 100 Ω resistor.

If one makes the extremely pessimistic assumption that APV inefficiency is dominated by 'ionization HIPs', with all APVs affected by more than 2 MeV of released energy being 10% inefficient in the following 30 bunch crossings, (i.e., half as inefficient as they are following a 'nuclear interaction HIP'), then $\eta_{\rm recovery}$ would be about 5%. However as the following Section shows, even in this case, the effects on track reconstruction would not be dramatic.

6.2 Tracking performances

One does not expect tracking efficiencies and resolutions to be significantly affected by the HIP problem. One track results usually from a fit to more than 11 points, and losing one does not

Layer	Single Muon (no HIP)	Single Muons	$b\bar{b}$
1	0.004 ± 0.001	0.013 ± 0.002	0.020 ± 0.002
3	0.003 ± 0.001	0.009 ± 0.002	0.019 ± 0.002
5	0.002 ± 0.001	0.014 ± 0.001	0.022 ± 0.002
9	0.001 ± 0.001	0.002 ± 0.001	0.007 ± 0.002

Table 10: *Hit inefficiency on signal tracks in single muon events and in $b\bar{b}$ events with transverse energy $E_T = 100$ GeV. As a reference, the second column shows results when HIP effects are not simulated. The results in the following two columns correspond to $\eta_{\text{recovery}} = 1\%$ in the first TIB barrel layer and are scaled accordingly to the average track-length per APV in the following layers. This value of η_{recovery} approximates to that measured for the 50 Ω resistor choice. Inside b jets the hit inefficiency is larger by about 1% because the probability of a HIP due to a signal track is not negligible in b jets.*

	No HIP	$\eta_{\text{recovery}} = 0.01$	$\eta_{\text{recovery}} = 0.05$
tracking efficiency			
100 GeV b-jets	0.87 ± 0.03	0.86 ± 0.03	0.82 ± 0.03
100 GeV u-jets	0.72 ± 0.03	0.70 ± 0.03	0.67 ± 0.03
b-tagging efficiency			
100 GeV b-jets	0.57 ± 0.04	0.56 ± 0.04	0.54 ± 0.04
100 GeV u-jets	0.045 ± 0.015	0.045 ± 0.015	0.045 ± 0.015

Table 11: *Effects of HIPs on tracking efficiency and b-tagging in b- and u-jets at high luminosity.*

affect the resolution on track parameters [8]. Furthermore, since during reconstruction a track is only lost if two consecutive hits are missing, the expected tracking inefficiency due to HIPs is only $\approx 10 \times \eta_{\text{tot}}^2$. According to Table 10, with a 50 Ω resistor, one expects a track inefficiency of only 0.1% for single muons and of 0.4% for b-jets tracks. If a 100 Ω resistor were used the inefficiency would reach 2% in b-jets.

This is verified by running standard CMS reconstruction algorithms on events produced with the ORCA HIP-simulation described in the previous sub-section. As Table 11 shows, there is minimal effect on the track reconstruction efficiency, even in the extreme case of $\eta_{\text{recovery}} =$ 5%. An important task of the CMS Tracker is the tagging of events with b or τ jets decaying hadronically. The tagging algorithms [8] make use of the good tracking efficiency and resolution of the Tracker, even inside collimated jets, and of the decay length in excess of 1 mm of the secondary vertexes. Table 11 also shows that these tags are insensitive to HIP effects.

6.3 Effect on the Expected CMS Tracker Data Rate

The mean numbers of fake clusters $N_{cluster}$ and fake strips N_{strip} produced per HIP, summed over all the bunch crossings following each HIP, are given in Table 6 of Sect. 4.1. They are broken down in several different ways to help understand what influences the fake rate. These results can be used to estimate the data rate per FED due to these fake clusters expected at CMS. If $\overline{P_{\rm hip}}$ is the probability of a HIP interaction occurring per APV per CMS event, $N_{APV} = 192$ is the number of APVs read by each FED, and $T = 10^5$ Hz is the L1 trigger rate, then the data rate per FED due to these fake clusters is given by:

$$\text{Rate (MB/s)} = T \times N_{apv} \times \overline{P_{\rm hip}} \times (2N_{\rm cluster} + N_{\rm strip})/(1024)^2$$

where 1 MB is defined as 2^{20} B. This follows from the fact that the FEDs will output 2 bytes of information per cluster (location of first strip and cluster width) and 1 byte for each strip in the cluster (8 bit ADC pulse height) [9].

Table 12 shows the data rate calculated for high luminosity p–p collisions in the innermost barrel layer. The variable $\overline{P_{\rm hip}}$ in this layer is taken from Eqn. 2. It is 9.3×10^{-4} if $\rm R_{inv} = 50\ \Omega$ or 12.7×10^{-4} if $\rm R_{inv} = 100\ \Omega$.

Table 12: *The expected data rate per FED due to fake clusters from non-uniform common-mode noise, which is expected at high luminosity in the innermost barrel layer of the CMS tracker. Results are subdivided according to the APV configuration and according to the value of the resistor* $\rm R_{inv}$. *They are also shown for two variants on the standard FED zero suppression algorithm. As explained in the text, one involves evaluating the common-mode noise for small groups of strips (e.g.* $\mathrm{C}M_{nstrips} = 16$*) whilst the other involves rejecting all wide clusters (e.g. requiring* $\mathrm{W}idth_{clus} < 10$*).*

$\rm R_{inv}$ (Ω)	APV config. Deconv.	Inv.	Zero Suppression variant	Fake data rate (MB/s/FED)
50	y	y	standard	3.3
50	y	y	$\mathrm{C}M_{nstrips} = 16$	0.3
50	y	y	$\mathrm{W}idth_{clus} < 5$	1.1
50	y	y	$\mathrm{W}idth_{clus} < 10$	1.6
100	y	y	standard	1.2
100	y	y	$\mathrm{C}M_{nstrips} = 16$	0.3
100	y	y	$\mathrm{W}idth_{clus} < 5$	0.7
100	y	y	$\mathrm{W}idth_{clus} < 10$	1.1
50	y	n	standard	1.8
100	y	n	standard	2.0
50	n	n	standard	6.2
100	n	n	standard	7.4
50	n	y	standard	6.9
100	n	y	standard	7.6

The fake data rate produced by HIPs, for the standard APV configuration and FED zero suppression algorithm, is only 3.3 (1.2) MB/s for the 50 (100) (Ω) resistor. This is small compared with the data rate of 103 MB/s [10] expected from signal and other noise sources. From this one can conclude that HIPs have no significant effect on the data rate. The more sophisticated FED zero suppression algorithms studied do reduce the fake data rate even further, but there is apparently no need for them (at least as far as this problem is concerned). Taking data in peak rather than deconvolution mode substantially increases the data rate to 6.9 (7.6) MB/s for the

50 (100) (Ω). However, this is not a major concern, since CMS will only run in peak mode for debugging and some calibration.

7 Summary

Highly Ionizing Particles (HIPs) produced by nuclear interactions in the tracker sensors are observed to produce large signals, which can momentarily saturate an APV readout chip. Detailed studies of this effect have been made using test-beam data taken at PSI and X5. In particular, the dependence of the results on the resistor value $\mathrm{R_{inv}}$ used in the power supply line to the APV inverter stage is measured, since this will influence the choice of this resistor.

Using data collected with random triggers at PSI, the probability of a 300 MeV/c pion producing a HIP on transversing 300 μm of silicon is measured. (This is the momentum of typical pions expected at CMS). It is in the range (4–10)$\times 10^{-4}$, depending on the severity of the ‘HIP’. Two independent analyses have been performed and the results are consistent. They are also compatible with an earlier X5 test-beam study of this effect [1]. The HIP production probability in 500 μm sensors is measured to be a factor of roughly $5/3$ higher, as expected. Interestingly, the rate seen when $\mathrm{R_{inv}} = 100\ \Omega$ is observed to be a factor 1.4 ± 0.4 larger than when $\mathrm{R_{inv}} = 50\ \Omega$.

The large HIP signal drives the APV baseline negative, as a result of the built-in tendency of the APV inverter stage to subtract any common-mode offset. The time evolution of the baseline is studied in special runs, where 30 successive data samples are read out at 25 ns time spacing following each HIP. The baseline recovers over a period of a few hundred nano-seconds. No significant dependence of the recovery time on sensor thickness is seen. However, the baseline recovers about 20% faster with $\mathrm{R_{inv}} = 50\ \Omega$ than with $\mathrm{R_{inv}} = 100\ \Omega$.

During the baseline recovery (which is equivalent to a large, negative common-mode offset), the common-mode offset is not flat across the 128 APV channels, but shows large distortions. This is a potential problem at CMS, since it is currently proposed that the FEDs will subtract the common-mode offset assuming that it is flat. Using the test-beam data, this is shown to lead to wide, fake clusters appearing in the data. However, in normal CMS running conditions, these are expected to increase the data rate by only 1.2% if $\mathrm{R_{inv}} = 100\ \Omega$. Curiously, this increases to 3.2% if $\mathrm{R_{inv}} = 50\ \Omega$, but this is still acceptably small. These numbers can be reduced, if necessary, by using more sophisticated algorithms in the FED.

By searching for tracks due to MIPs during the 30 bunch crossings following a HIP, one can measure the efficiency of the tracker. This simply involves checking in which wafers a hit is associated to each reconstructed track. In APVs not affected by the original HIP, the efficiency is measured to be close to 100%. However, in APVs affected by the HIP, the efficiency is close to zero immediately following the HIP, recovering over a few hundred nano-seconds. Even after 30 bunch crossings (750 ns) it does not recover completely. The mean inefficiency over this period is 21 ± 2% with $\mathrm{R_{inv}} = 50\ \Omega$ and 38 ± 3% with $\mathrm{R_{inv}} = 100\ \Omega$ (with some dependence on the HIP severity).

Results on the HIP probability per incident particle and on the mean APV inefficiency following a HIP, have been combined with Monte Carlo estimates of particle fluxes at CMS, to predict the expected inefficiency due to HIPs in the CMS Tracker. In the innermost barrel layer, where the effect should be largest, the hit inefficiency is 1.9 ± 0.2% for $\mathrm{R_{inv}} = 100\ \Omega$ and 0.8 ± 0.1% for

$\mathrm{R_{inv}} = 50\ \Omega$.

8 Acknowledgments

We thank the hospitality of the proton accelerator at the Paul Scherrer Institut, Villigen, Switzerland, where this work was performed. We also thank F. Bosi and P. Tempesta for their support in building the TIB modules, L. Berretta for the mechanics of the supporting boxes, M. Ageron and C. Girerd for their precious help on TSC modules, A. Honma for his invaluable help in preparing the modified resistors, J. Martin and J. Hill for the PSI setup installation, S. Tkaczyk, L. Spiegel and L. Christofek for building and testing TOB module at Fermilab.

References

[1] *"Information on Oct. 2001 X5 Test-Beam"*,
http://hepwww.rl.ac.uk/CMSTracker/b_tau/TestBeam/X5oct2001.html,
R. Bainbridge *et al.*, *"The Effect of Highly Ionising Events on the APV25 Readout Chip"*, CMS NOTE 2002/038.

[2] M. Raymond, *"Laboratory studies of the HIP and pin-hole effects on the APV25"*,
http://cmsdoc.cern.ch/Tracker/managment/Agenda_GTM/GM_01_12/Mark_CMShipstalk.ppt (Dec. 2001),
http://cmsdoc.cern.ch/ ghall/TKEL_0102/Raymond_0102.pdf (Jan. 2002).

[3] *"ORCA Test-Beam Software"*,
http://hepwww.rl.ac.uk/CMSTracker/b_tau/TestBeam/tbeam_software.html

[4] *"ORCA User Guide"*,
http://cmsdoc.cern.ch/swdev/snapshot/ORCA/UserGuide/html/UserGuide.html

[5] RAL Micro-Electronics Group, "APV25 User Guide",
http://www.te.rl.ac.uk/med/projects/High_Energy_Physics/CMS/APV25-S1/pdf/User_Guide_2.0.pdf

[6] M. Huhtinen, *"Highly Ionising Events in Silicon Detectors"*, CMS-NOTE-2002/011.

[7] L. Mirabito, Note in preparation

[8] *"CMS Data Acquisition and Higher Level Trigger TDR"*, CERN/LHCC 02-26.

[9] K.W Bell *et al.*, *"User Requirements Document for the final FED of the CMS Silicon Strip Tracker"*, CMS-NOTE-2001/043, Sections. 8 and 9.

[10] O. Kodolova, I. Tomalin, P. Yepes, *"Expected Data Rates from the Silicon Strip Tracker"*, CMS-NOTE-2002/047.